NASA TECHNICAL REPORT

NASA TR R-449

NASA TR R-449

TESTING OF PRINTED CIRCUIT BOARD SOLDER JOINTS BY OPTICAL CORRELATION

Patrick N. Espy

George C. Marshall Space Flight Center
Marshall Space Flight Center, Ala. 35812

NATIONAL AERONAUTICS AND SPACE ADMINISTRATION • WASHINGTON, D. C. • NOVEMBER 1975

1. REPORT NO.	2. GOVERNMENT ACCESSION NO.	3.
NASA TR R-449		

4. TITLE AND SUBTITLE	5. REPORT DATE
Testing of Printed Circuit Board Solder Joints by Optical Correlation	November 1975
	6. PERFORMING ORGANIZATION CODE
7. AUTHOR(S)	8. PERFORMING ORGANIZATION REPORT #
Patrick N. Espy	M153
9. PERFORMING ORGANIZATION NAME AND ADDRESS	10. WORK UNIT NO.
George C. Marshall Space Flight Center Marshall Space Flight Center, Alabama 35812	11. CONTRACT OR GRANT NO.
	13. TYPE OF REPORT & PERIOD COVERED
12. SPONSORING AGENCY NAME AND ADDRESS	
National Aeronautics and Space Administration Washington, D.C. 20546	Technical Report
	14. SPONSORING AGENCY CODE

15. SUPPLEMENTARY NOTES

Prepared by Space Sciences Laboratory, Science and Engineering

16. ABSTRACT

An optical correlation technique for the nondestructive evaluation of printed circuit board solder joints has been evaluated. Reliable indications of induced stress levels in solder joint lead wires are achievable. Definite relations between the inherent strength of a solder joint, with its associated ability to survive stress, are demonstrable.

17. KEY WORDS	18. DISTRIBUTION STATEMENT
Nondestructive testing Fourier optics Coherent optics	Category 74

19. SECURITY CLASSIF. (of this report)	20. SECURITY CLASSIF. (of this page)	21. NO. OF PAGES	22. PRICE
Unclassified	Unclassified	90	$4.75

MSFC - Form 3292 (Rev December 19

For sale by the National Technical Information Service, Springfield, Virginia 22161

TABLE OF CONTENTS

LIST OF ILLUSTRATIONS

LIST OF ILLUSTRATIONS (Concluded)

LIST OF TABLES

TESTING OF PRINTED CIRCUIT BOARD SOLDER JOINTS BY OPTICAL CORRELATION

I. INTRODUCTION

The reliability of electronic system components was not of substantial concern when such components were relegated solely to noncritical commercial and military applications. Reliability of system components became more critical with the advent of orbital and deep space probes. The weight problem of redundant subsystems necessitated the acceptance of the design philosophy in which each system, subsystem, and component would operate with a minimum probability of failure over the projected life of the system. Manned space flight introduced yet another factor that elevated the reliability requirements of components used.

These evolving reliability criteria required systems analysts to focus considerable attention on the electronic components and the circuit boards to which they were mounted. Survival of the electronic components in the high-vibration-level environment necessitated encapsulation of the printed circuit board in a conformal coating. These encapsulating materials somewhat accentuate the problem of component survival. As a result of the differing coefficients of thermal expansion of materials constituting printed circuit boards, significant stress levels may be attained during temperature changes. The levels of the stresses attained and the resulting damages depend primarily on the design of the printed circuit board. For poorly designed boards, a temperature change of a few degrees has been known to cause failures.

A program to develop designs that minimize the effect of thermal variations was initiated once the source of the failures was recognized. Materials with the lowest possible differences in coefficients of thermal expansion were chosen for conformal coatings, printed circuit boards, and other components. Use was made of minimum thickness coatings, stress relief in electronic component leads, and expansion absorbing spacers. The problem of thermally induced solder joint fracture was minimized by taking these precautions. However, after all efforts were made, there remained a residual failure rate among solder joints. The approach of attempting to identify faulty solder joints was undertaken at this time.

Severe restrictions are imposed upon the testing of space-flight-qualified units. These restrictions prevent any degradation of the performance of the system components. The severity of thermal tests is restricted as is the case with vibration, electromagnetic susceptibility, and other types of qualifying tests. Because solder joints on printed circuit boards may be subjected to only a small temperature variation without degradation, an extremely sensitive observational technique is required to measure the physical changes. This report presents the details of a study of the feasibility of nondestructive evaluation

of solder joints by optical correlation. This study assumes the existence of a definable relationship between the physical changes induced by temperature variations and a propensity towards failure. Optical correlation techniques were assumed capable of both measuring these changes and establishing the relationship indicated.

The type of failure of interest in this study is the cracking of solder material or its separation from the lead wire in a printed circuit board joint which results from repeated stressing of the material. Solder joint failure occurs if the stress exceeds the yield strength of the solder. However, stress levels well below the yield strength of the material will cause failure after a number of stress cycles.

The relationship between the failure characteristics of solder joints and optical correlation measurements is assumed to be determinable from a practical number of experimental measurements. For a practical system it is desirable that the data be such that a statistical analysis is not necessary.

For a nondestructive evaluation technique to be feasible, it must be based on the existence of a phenomenon or a parameter that is reliably indicative of latent weaknesses or incipient failure. Furthermore, the phenomenon or parameter must be economical and technically measureable.

Solder, when applied to electrical connections, is used in such a manner that it is not required to withstand large static shear or tensile forces. Instead, it yields under force in a plastic manner and thus accommodates internal stresses. Failure of a solder connection normally occurs as a fatigue failure after the solder has plastically yielded a number of times. It is this deformation in solder joints that is the measurable quantity in the nondestructive technique of optical correlation.

A system was developed to perform optical correlation measurements on solder joints. Only through the development of a high efficiency temporally stable holographic filter was this possible. During the analysis of the mechanical stability of the measuring system and observation of the performance characteristics, a new measurement technique was discovered. This technique utilizes optical correlation for the nonperturbing measurement of acoustics in solder joints. In general, surface vibrations may be measured up to the frequency limit of the photodetector. This technique is the subject of a patent application presently in process.

During the studies reported here, a process evolved that produced higher efficiency holograms with increased long term stability. The improvements attained were the result of generating a composite amplitude attenuation and phase hologram by special treatment of a typical amplitude attenuation hologram. Since no mathematical description that defines the transmittance of an amplitude-phase hologram has been published, a derivation is included in this report.

II. LITERATURE SURVEY

The advent of printed circuit boards was followed by a concern for the reliability of solder joints connecting components to printed circuit boards and feed-through connections from one side of the board to the other. Lockheed Missiles and Space Company [1] reported on an investigation of solder joints in circuit boards in November, 1960. The Military Electronics Computer Division of Burroughs Corporation [2] published the results of an evaluation of the plated-through hole type of printed circuit board connection in 1962; this evaluation included environmental testing. A Boeing Company report [3] defined defects that occur in printed circuit board joints and illustrated them by type. A study by NASA-Marshall Space Flight Center [4] also examined the causes and manifestations of cracked solder joints.

Two extensive industrial studies were subsequently conducted utilizing data and failure mode information previously acquired [5,6]. These studies included extensive testing of circuit board joints to extend the information previously acquired. The tests were principally thermal in nature with slow, cyclic tests and thermal shock tests being made. Classifications of failures were further refined to better describe the failures and to more directly indicate the causes. Various configurations of solder joints were tested to verify theoretical modes of failure. Basic metallurgical studies yielded an understanding of the physical properties of various solders, their wetting characteristics, contamination embrittlement, thermal effects, crystalline structures, their ability to bond with copper, and related areas. These studies provided an in-depth understanding of a wide range of problems and performances of solder joints on printed circuit boards.

Three studies concentrated on the nondestructive evaluation of solder joints [7-9]. The techniques of thermal radiation, radiography, ultrasonics, fluoroscopy, phosphorescence, and infrared photography were all considered in these reports. Only standard visual inspection procedures have found general acceptance. Visual inspection usually includes both low and high magnification observations. One disadvantage of this approach is the subjective nature of visually evaluating a solder joint. Radiography has found a limited acceptance, but it is not generally applicable to inspection of complex circuit boards. The other nondestructive techniques suffer from limited applicability, problems of interpretation, or both.

Several researchers [10-13] have applied optical correlation techniques to the detection of fatigue, impending failure, or strain in materials. The ability to detect strains [12] results from the high sensitivity of optical correlation systems to the lateral movement of the object under test. References 10, 11, and 13 provide information about an unique approach to determining surface changes. Fatigue failure can be predicted to a high degree of reliability from surface condition measurements. It is significant that optical correlation measurements are able to detect surface changes that cannot be detected with optical microscopic inspection. Large surface areas, relative to the detectable changes, may be observed.

Another study [14], performed at Marshall Space Flight Center, employed optical correlation measurements to evaluate solder joints. This effort was based on the determination of minute changes in the condition of solder joints under test. These changes were permanent and the method of testing could not be considered nondestructive in nature. This optical system was refined for obtaining data for this report. However, innovative testing methods were developed to provide nondestructive evaluation of solder joints.

III. THEORY

A. Wavefront Recording

Conventional photographic imagery involves recording the intensity of a wavefront of electromagnetic radiation on sensitized material. The development of coherent sources of radiation modified this concept by permitting the recording of both the amplitude and phase of wavefronts of electromagnetic radiation by mutual interference. Given the ability to record and to reproduce this information, the reconstruction of a wavefront becomes possible. This process is called holography. Coherent sources here are meant to imply convenient, controllable sources of at least one discrete wavelength, that wavelength not varying more than a small fraction of its nominal value. The laser satisfies these criteria.

Consider the representation of an electromagnetic radiation wavefront:

$$\nabla^2 U - \frac{1}{c^2} \frac{\partial^2 U}{\partial t^2} = 0 \quad . \tag{1}$$

A solution in time and position of this wave equation is [15]

$$U = A'(x,y,z) \exp \{i[\phi(x,y,z)] + \omega t\} + A''(x,y,z) \exp \{i[\phi(x,y,z)] - \omega t\} \quad . \tag{2}$$

The terms in equation (2) are defined with regard to the orthogonal coordinates (x, y, z) and time, t. The functions A and ϕ are real functions and U is complex. The function A is the amplitude of the solution to the wave equation and ϕ is the phase function. The time dependence of the radiation wavefront is cancelled in the process of obtaining the intensity of the sum of two coherent wavefronts. The radiation sensitive material records the sum of the two wavefronts which are represented by position dependent functions. The wavefronts, designated U_1 and U_2 in Figure 1, intersect at the recording medium

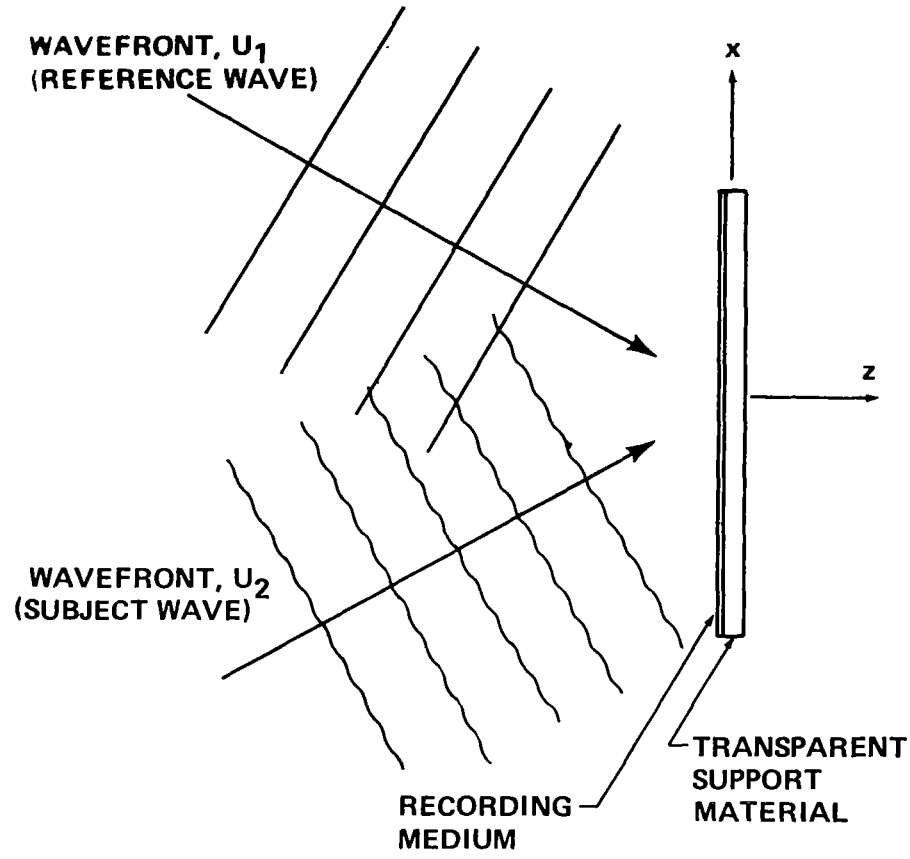

Figure 1. Holographic recording of interfering wavefronts.

positioned in the (x,y) plane perpendicular to the z-axis. The amplitude and phase relationship of the two wavefronts as functions of position are

$$U_1 = A_1(x,y) \exp[i\phi_1(x,y)] \tag{3}$$

and

$$U_2 = A_2(x,y) \exp[i\phi_2(x,y)] \quad , \tag{4}$$

respectively. The sum of the amplitude and intensity functions of these wavefronts are given respectively as

$$U_{sum} = U_1 + U_2 \tag{5}$$

and

$$I_{sum} = (U_1 + U_2)(U_1^* + U_2^*) \tag{6}$$

$$I_{sum} = |U_1|^2 + |U_2|^2 + U_1^* U_2 + U_1 U_2^* \quad . \tag{7}$$

Here U_{sum} and I_{sum} are the amplitude and intensity functions and the asterisk signifies the complex conjugate. The amplitude functions are complex quantities and are summed as such.

The amplitude functions mentioned previously may be recorded as either amplitude attenuation or phase recordings. Amplitude attenuation recordings may be defined as those photographically generated recordings whose optical density will vary spatially as a function of the exposure. These photographic transparencies are employed in a manner such that a wavefront incident on the transparency is modulated by the optical density information as the wavefront passes through. These recordings may be treated as planar or volume type holograms depending upon the thickness of the photographically sensitive material and the angle between the two wavefronts.

The relationship between the density of the transparency and the exposure is most often presented as the Hurter and Driffield characteristic curve (Fig. 2a) or, more recently, as the amplitude transmittance versus exposure curve (Fig. 2b). Because of the nature of holographic work, the latter presentation is more useful, whereas the Hurter and Driffield curve is more useful in standard photographic applications. From the amplitude transmittance versus exposure curve the following approximation for the representation of the linear portion is apparent:

$$T_a = T_0 - k_1 E \quad , \tag{8}$$

where T_a is the amplitude transmittance, E is the exposure, and T_0 and k_1 are appropriate constants. Exposure is the product of the light intensity, I, and the exposure time, t. The wavefront transmitted through a transparency will be modulated by the amplitude transmittance of the transparency,

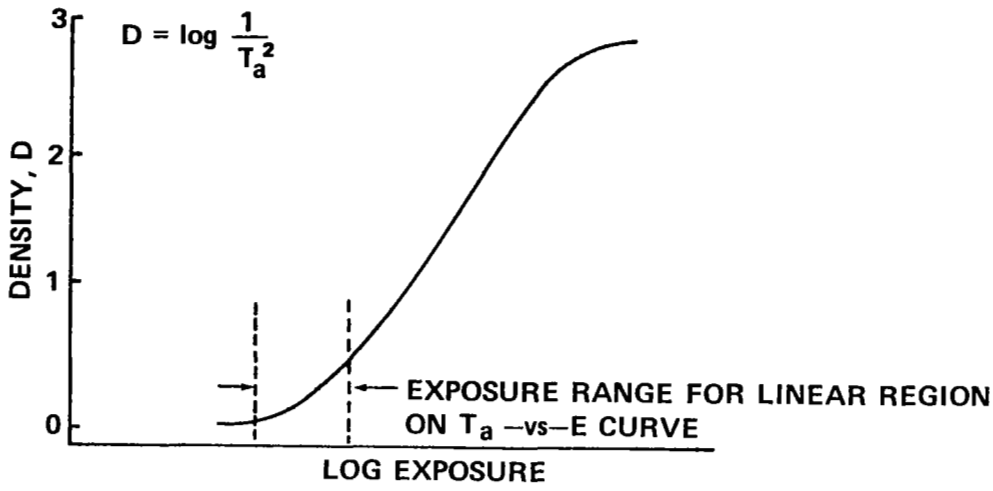

a. Hurter and Driffield curve.

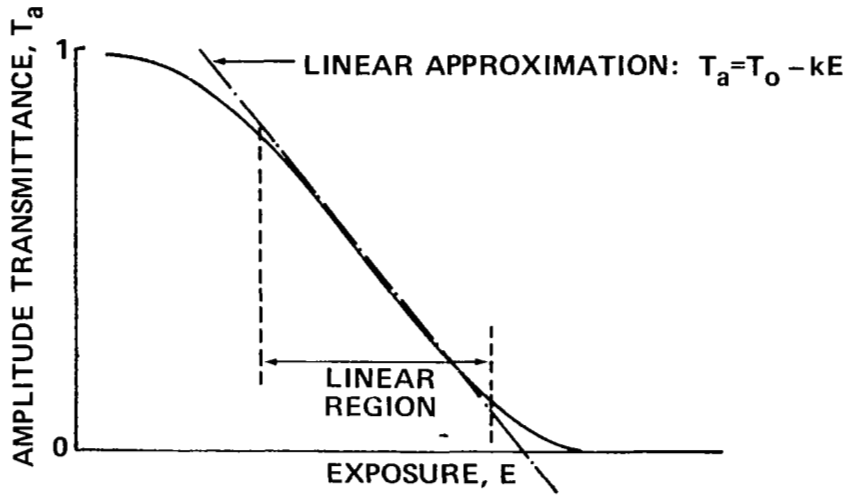

b. Amplitude transmittance versus exposure curve.

Figure 2. Sensitometric characteristics of recording medium (photographic emulsion).

$$W_o = T_a W_{in} \tag{9}$$

$$= T_o W_{in} - k_1 E W_{in} \quad , \tag{10}$$

where W_{in} and W_o are the input and output functions of the transparency.

Phase recordings are those in which the information stored is retrieved in the phase shifts that occur as a wavefront passes through various locations of the recording. The phase shift information is produced by the wavefronts incident upon the recording material during exposure. The materials employed in phase recordings, and to some extent the materials employed in attenuation recordings, are developed in such a manner that either the thickness, the index of refraction, or both are functions of the incident light intensity. In either case, the input wave function, in passing through the material is multiplied by a variable phase shift factor exp [iKE(x,y)]. The factor K is the constant of proportionality relating the exposure to the phase shift. The desired linearity in the developed recording is achieved in the design of the developing process.

The presence of both attenuation and phase shift is the rule instead of the exception since it is difficult to eliminate phase information in most photosensitive materials [16]. Surface relief results from removal of the undeveloped silver halides in the development of silver halide emulsions. Exposure-dependent changes of the index of refraction occur in the silver halide emulsion. The thickness variations become significant at spatial frequencies less than 100 lines per millimeter [17]. The optical system employed for this study minimized surface relief effects by generating spatial frequencies greater than 1000 lines per millimeter.

B. Wavefront Reconstruction

The wavefront reconstructed by a hologram may be either of the two wavefronts present during the recording of the hologram. Either of the wavefronts may be re-created by impinging the other on the developed hologram.

Attenuation holograms reconstitute a wavefront by the spatial variation in attenuation of another wavefront as it passes through the recording plane. The amplitude attenuation is a function of the relative powers of the two light beams during exposure, the characteristics of the photosensitive material, the developing process, and other factors. The two beams employed in a holographic recording are denoted as the subject beam, S, and the reference beam, R. These light beams are defined as

$$S = S_o(x,y) \exp [i\phi_s(x,y)] \tag{11}$$

and

$$R = R_o(x,y) \exp [i\phi_r(x,y)] \quad . \tag{12}$$

$S_o(x,y)$ and $R_o(x,y)$ are real functions of the amplitude of the optical signal in the (x,y) plane of the recording material. The phase angles, like the amplitudes, are defined in terms of position in the (x,y) plane. The transmission function of an amplitude transmittance hologram is then

$$T_a = T_0 - k_1 E = T_0 - k_1 It \tag{13}$$

$$= T_0 - k_1(|S|^2 + |R|^2 + SR^* + S^*R)t \quad , \tag{14}$$

where t is the exposure time, I is the total light intensity, and T_0 and k_1 are constants dependent upon the recording material and developing process. The reconstruction of S is obtained by impinging the reference beam, R, on the hologram. The total light distribution resulting from impinging the reference beam on the hologram may be expressed mathematically as

$$RT_a = RT_0 - Rk_1 It \tag{15}$$

$$= RT_0 - k_1 t(|S|^2 + |R|^2 + SR^* + S^*R)R \tag{16}$$

$$= RT_0 - k_1 t[(|S|^2 + |R|^2)R + (S|R|^2 + S^*R^2)] \quad . \tag{17}$$

Of the resulting expression only the term $(-k_1 t|R|^2 S)$ is of interest since it is the only term that accurately reproducts the subject beam. The other terms containing S discard or modify the phase term. Impinging S onto the hologram produces the R wavefront in a similar manner.

Reconstruction of the subject wavefront may be obtained by employing a phase hologram in a manner similar to that discussed for attenuation holograms in the previous paragraph. The output intensity from phase holograms is equal to the input intensity but

is shifted in phase. This type of hologram has a phase transmission function represented by

$$T_p = \exp[i\phi(x,y)] = \exp[ik_2E(x,y)] \quad . \tag{18}$$

The phase shift, $\phi(x,y)$, is induced by either a refractive index change or hologram thickness change; k_2 is a constant of proportionality. No relative phase shift occurs in the impinging wavefront for uniform thickness and refractive index; therefore, constant phase shift factors may be ignored.

For phase holograms that are linear with exposure, the phase transmission function is approximated as

$$T_p = \exp(ik_2It) \tag{19}$$

$$= \exp[ik_2t(|S|^2 + |R|^2 + SR^* + S^*R)] \tag{20}$$

$$T_p = \exp[ik_2t(|S|^2 + |R|^2)]\left[\exp\left(ik_2tS_oR_o\{\exp[i(\phi_s - \phi_r)] + \exp[-i(\phi_s - \phi_r)]\}\right)\right] \tag{21}$$

$$= \exp[ik_2t(|S|^2 + |R|^2)] \exp\{2ik_2tS_oR_o[\cos(\phi_s - \phi_r)]\} \quad . \tag{22}$$

To properly utilize equation (22) the exponential term containing the cosine function must be expanded. The equivalent series expansion of Bessel functions of the first kind is as follows:

$$\exp(i\alpha\cos\beta) = J_0(\alpha) + 2\sum_{n=1}^{\infty}(-1)^nJ_{2n}(\alpha)\cos 2n(\beta)$$

$$= 2i\sum_{n=0}^{\infty}(-1)^{n+2}J_{2n+1}(\alpha)\,(2n+1)\beta \quad , \tag{23}$$

where α and β are arbitrary values and J_i is the Bessel function of order i. Since it is desired to observe only the first order diffraction image corresponding to the cos(β) term, the n = 0 term of the complex function series of equation (23) is retained while all other terms are discarded. As a result, T_p can be written as

$$T_p = \exp\,[ik_2t(|S|^2 + |R|^2)]\,2iJ_1(2k_2tS_oR_o)\cos(\phi_s - \phi_r) \quad . \tag{24}$$

The Bessel function $J_1(2k_2tS_oR_o)$ or $J_1(\alpha)$ may be expanded into the series

$$J_1(\alpha) = \frac{\alpha}{2} - \frac{\left(\frac{\alpha}{2}\right)^3}{1^2 \cdot 2} + \frac{\left(\frac{\alpha}{2}\right)^5}{1^2 \cdot 2^2 \cdot 3} - \cdots \tag{25}$$

from the relationship [18]

$$J_n(\alpha) = \left(\frac{\alpha}{2}\right)^n \sum_{k=0}^{\infty} \frac{(-1)^k}{k!\Gamma(n + k + 1)} \left(\frac{\alpha}{2}\right)^{2k} \qquad |\arg \alpha| < \pi \quad . \tag{26}$$

Only the first series expansion term is significant for sufficiently small α. Equation (24) may now be written to a good approximation as

$$T_p = i\left\{\exp\,[ik_2t(|S|^2 + |R|^2)]\;2k_2tS_oR_o\,\cos(\phi_s - \phi_r)\right\} \tag{27}$$

$$T_p = k_2tS_oR_o \exp\left\{i\left[k_2t(|S|^2 + |R|^2) + \frac{\pi}{2}\right]\right\}\left\{\exp\,[i(\phi_s - \phi_r)] + \exp\,[-i(\phi_s - \phi_r)]\right\} \tag{28}$$

$$= k_2t \exp\left\{i\left[k_2t(|S|^2 + |R|^2) + \frac{\pi}{2}\right]\right\}\left\{SR^* + S^*R\right\} \quad , \tag{29}$$

since

$$i = \exp\,(i\pi/2) \quad . \tag{30}$$

Equation (29) is to be compared with equation (14) for amplitude transmittance. As in the case of the amplitude transmittance hologram, the phase hologram may be used to reconstruct either the subject or reference beam.

In holograms in which both amplitude and phase modulation occur, the total transmittance will be

$$T_t = T_a T_p \quad . \tag{31}$$

Only the first order terms in S and R in the product $T_a T_p$ are useful because they alone provide first order images. The first order images result from using constant terms and first order terms in both T_a and T_p. That is,

$$T_a(C + F)T_p(C + F) = T_a(C)T_p(F) + T_p(C)T_a(F) + C + H \quad , \tag{32}$$

where C denotes constant terms, F denotes first order terms, and H denotes higher order terms. The first order term in T_a is $(-k_1 t)\,(SR^* + S^*R)$ and the constant term is T_0. For reference beams with plane wavefronts, $-k_1 t|R|^2$ is also constant, but a more general R will be considered here. The first order term of T_p is

$$k_2 t \exp\left\{i\left[k_2 t(|S|^2 + |R|^2 + \frac{\pi}{2}\right]\right\}\left\{SR^* + S^*R\right\} \quad .$$

The constant term in T_p arises from the $J_0(2k_2 t S_o R_o)$ term of equation (23). Expansion of $J_0(\alpha)$ yields

$$J_0(\alpha) = 1 - \frac{\left(\frac{\alpha}{2}\right)^2}{1^2 \cdot 2} + \frac{\left(\frac{\alpha}{2}\right)^4}{1^2 \cdot 2^2 \cdot 3} - \cdots \quad , \tag{33}$$

where α is $2k_2 t S_o R_o$. For sufficiently small α the Bessel function, J_0, is approximately unity. The total transmittance function of the first order S and R terms is

$$T_t = -k_1 t(SR^* + S^*R)(1) + T_0 k_2 t \exp\left\{i\, k_2 t(|S|^2 + |R|^2) + \frac{\pi}{2}\right\} (SR^* + S^*R) + C + H \tag{34}$$

$$T_t = \left\{ T_0\left(k_2 t \exp\left\{i\left[k_2 t(|S|^2 + |R|^2) + \frac{\pi}{2}\right]\right\}\right) - k_1 t \right\}\left\{SR^* + S^*R\right\} + C + H \tag{35}$$

where C denotes constant terms and H denotes terms higher than first order. Letting $G_a = k_1 t$ and letting

$$G_p = T_0 k_2 t \exp\left\{i\left[k_2 t(|S|^2 + |R|^2) + \frac{\pi}{2}\right]\right\} \quad , \tag{36}$$

then

$$T_t = (G_p - G_a)(SR^* + S^*R) + f(n) \quad , \tag{37}$$

where f(n) is other than first order terms in S and R. The terms G_p and G_a are representative of the modulation characteristics of the hologram. The first order terms in S and R will exhibit either reinforcement or cancellation depending upon the relative values of G_p and G_a, that is, upon the relative contributions of the phase and attenuation effects in the hologram. These relative contributions are determined by the exponential term which depends upon the thickness and response of the photosensitive material.

C. Fourier Holography

The holograms employed as filters in this study are Fourier holograms (the complex recordings of Fraunhofer diffraction patterns), since the nominal Fourier transform is recorded. In contrast, holograms normally used for image reconstruction are complex recordings of Fresnel diffraction patterns. For systems with transparencies as subjects, the conditions for Fraunhofer diffraction are realized when the subject-to-illuminator separation and the subject-to-hologram separation are large and the ratio of wavelength to minimum subject feature size is small. Fourier holograms can be constructed with short subject to hologram distances by placing a lens in the near field (Fresnel region) of the subject. The lens synthesizes a large subject-to-hologram distance. In practical applications the subject plane is one focal length in front of the lens; the hologram is located one focal length behind the lens. The source may be considered to be

infinitely separated from the subject when parallel illumination is utilized. However, unless a front-illuminated subject is planar and specularly reflecting, the infinite source separation approximation must be considered in more detail.

The subject under consideration in this study was a solder joint on a printed circuit board. The configuration of the joint varied from approximately conical to hemispherical. Surface conditions ranged from smooth and shiny to dull and rough, which produced varying reflecting characteristics. The total output from the solder joint may be described as a diffusely scattered background with specular reflections. The specular reflection component of the optical output from the solder joint varied from a few percent to approximately half of the total output.

The surface condition of solder is affected by the temperature achieved in the soldering procedure, the composition and rate of cooling of the solder, and any mechanical movement of the tin-lead eutectic during solidification of the solder joint. A properly formed solder joint is a specular reflector. A poorly formed solder joint or one which has been stressed is a diffuse reflector as a result of crystal formation in the solder. As the crystal sizes decrease because of further stress, the reflected light contains less specular content and more diffuse content. In the limit, the crystal is a point scatterer. The light reflected from the solder joint may be considered as a composite of wavefronts transmitted by transparencies that are illuminated from the rear. The wavefronts from the transparencies correspond to the wavefronts from the specularly reflecting crystal faces of the solder. By the principle of superposition, the total subject wavefront may now be described as the sum of wavefronts.

When the subject is at the front focal plane of a lens, the light distribution in the rear focal plane is the Fourier transform of the subject, accurate within a constant and a phase factor [16]. A point source of light located in the front focal plane of a lens produces a uniform light distribution in the back focal plane; this is analogous to the Fourier transformation of a Dirac delta function into a uniform distribution in the frequency domain. Conversely, a plane wavefront in the front focal plane produces, by Fourier transformation, a point distribution (delta function) in the back focal plane. A transparency, containing optical density information, illuminated by a parallel beam produces a point of light surrounded by a spatial distribution of light, where the distance from the central point is proportional to the spatial frequency of the subject features. As a result of these relationships, a lens may be said to perform a Fourier transformation and the back focal plane may be called the spatial frequency plane. When the illuminating beam is not parallel to the optical axis of the system, the central image point is displaced from the optical axis in the spatial frequency or Fourier transform plane. The light distribution in the spatial frequency plane can be described as the superposition of the Fourier transforms of numerous transparencies, with the angle of illumination and the size of the subjects dependent upon the orientation and size of the surface elements of the solder.

The upper spatial frequency limit of a Fourier lens is normally specified in terms of a plane wave modified only by diffraction from the elements in the subject transparency. Because the crystal faces in the solder joint are oriented at different angles, there will be no unique zero frequency point in the spatial frequency plane and no unique Fourier lens spatial frequency bandpass. Every point in the spatial frequency plane can contain components from many elements of the solder joint. Therefore, it is not reasonable to define a spatial frequency limit for this system. This condition is one of several characteristics of this optical system which differs from most systems that have been considered and analyzed in the open literature. It is necessary, therefore, to consider the more general optical Fourier transform theory instead of the specialized treatments usually presented in the literature.

The Fourier transform lens employed in this system (Fig. 3) was located one focal length in front of the subject while the recording plane was located one focal length behind the lens. The light distribution in the recording plane was not precisely a Fourier transform since the recording medium was not perpendicular to the optical axis of the transform lens.

It should be noted here that according to the Fraunhofer-Kirchoff theory, a wavefront is converted into the Fourier transform of that wavefront as the distance it has traveled approaches infinity. In practical applications a finite distance is sufficient for a wavefront to take on a Fourier transform characteristic[1] if the distance is large compared to the size of the diffracting elements and the wavelength of the illuminating light. During the experimental procedures of this study, the transform lens was removed from the system and successful optical correlation measurements were made, the hologram being a recording of a lensless Fourier transform. The successful measurement of optical correlation, therefore, was not dependent upon an exact recording or reconstruction of the Fourier transform of the subject.

The representation of the subject beam as recorded in the photographic medium is approximated by

$$S(x_2,y_2) = \mathfrak{F}[s(x_1,y_1)] \quad , \tag{38}$$

where $s(x_1,y_1)$ is the wavefront reflected from the subject, $\mathfrak{F}$ indicates the Fourier transform, x_1 and y_1 are coordinates in the subject plane, and x_2 and y_2 are coordinates in the spatial frequency plane. Furthermore,

$$s(x_1,y_1) = s_o(x_1,y_1) \exp i\psi_s(x_1,y_1) \quad , \tag{39}$$

1. Private communications with A. Vander Lugt.

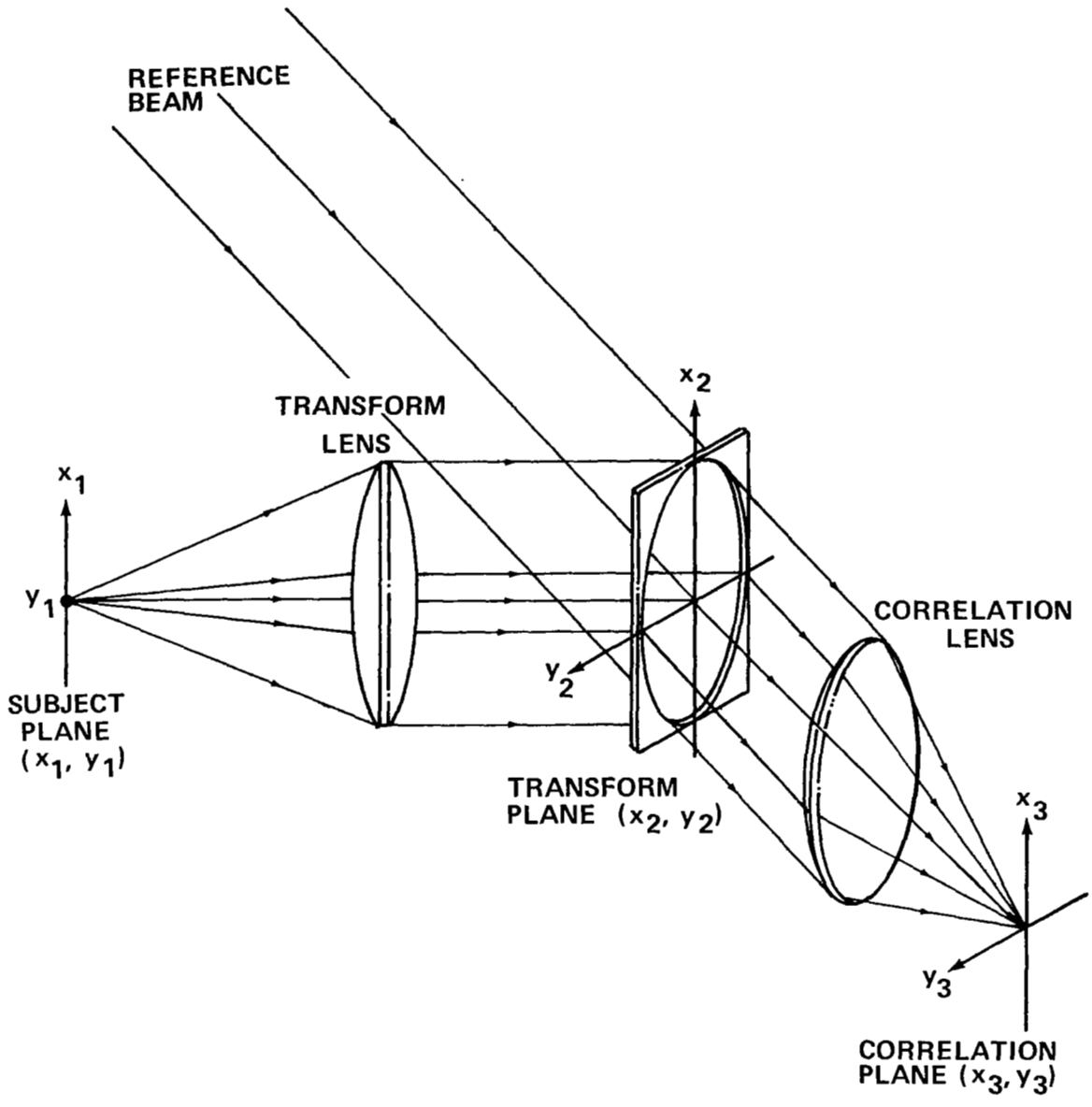

Figure 3. Optical correlation system with coordinate references.

where $s_o(x_1,y_1)$ and $\psi_s(x_1,y_1)$ are real amplitude and phase terms respectively. Similarly,

$$S(x_2,y_2) = S_o(x_2,y_2) \exp i\phi_s(x_2,y_2) \quad , \tag{40}$$

where $S_o(x_2,y_2)$ and $\phi_s(x_2,y_2)$ are amplitude and phase terms.

The reference beam, with which the subject beam interferes at the recording plane, is represented by

$$R(x_2,y_2) = R_o(x_2,y_2) \exp i\phi_r(x_2,y_2) \quad . \tag{41}$$

As a first approximation the reference beam is a uniform, planar beam. Therefore, at the recording plane the value of $R_o(x_2,y_2)$ is constant, since the amplitude is independent of the (x_2,y_2) position. The phase term is independent of x_2 and linear in y_2; however, the expression $\phi_r(x_2,y_2)$ will be retained for generality.

The combination of the subject and reference beams in the (x_2,y_2) plane yields the amplitude term

$$U = S(x_2,y_2) + R(x_2,y_2) \tag{42}$$

$$= S_o(x_2,y_2) \exp i\phi_s(x_2,y_2) + R_o \exp i\phi_r(x_2,y_2) \quad . \tag{43}$$

The intensity corresponding to this amplitude expression is

$$I = |S(x_2,y_2) + R(x_2,y_2)|^2 \tag{44}$$

$$I = SR^* + S^*R + SS^* + RR^* \tag{45}$$

$$= SR^* + S^*R + |S|^2 + |R|^2 \tag{46}$$

$$= S_o(x_2,y_2)R_o(x_2,y_2)\{\exp[i(\phi_s - \phi_r)] + \exp[-i(\phi_s - \phi_r)]\} + |S|^2 + |R|^2 \, . \tag{47}$$

The shape of the amplitude transmittance versus exposure curve (Fig. 2b) requires a certain bias exposure before the linear region of the curve is reached. The intensity of the reference beam alone is sufficient for operation on the linear portion of this curve. The subject beam need be only a fraction of the reference beam intensity to assure linear

modulation of the reference bias exposure by the desired signal ($SR^* + S^*R$). For practical applications, the reference beam intensity should be 2 to 2.5 times the subject beam intensity. For phase holograms, the phase modulation of the recording medium is optimized by a bias phase shift of at least π. This bias extablishes operation in the linear range of exposure [19].

Fourier transform functions are integral parts of the recorded information as shown in equation (47). Also, the phase of the subject and reference beams is contained in the intensity sensitive recording material. This recording of the phase information allows for the wavefront reconstruction by a hologram.

D. Optical Correlation

The purpose of recording holograms is the reconstruction of optical wavefronts. These reconstructed wavefronts may be used for observation, for comparing a subject under test with the original configuration of the subject through interference, or for a number of other purposes. This particular application involves the reconstruction of the planar reference beam because of amplitude information contained in that beam. This process is called optical correlation. The reconstruction is accomplished by illuminating the developed hologram with the subject beam. Initially, the subject beam will be considered to be unchanged from the subject beam configuration existing during the exposure time of the hologram.

As previously shown by equation (35), the total transmittance of a hologram is

$$T_t = \left\{ T_0 \left(k_2 t \exp\left\{ i \left[k_2 t(|S|^2 + |R|^2) + \frac{\pi}{2} \right] \right\} - k_1 t \right) \right\} \left\{ SR^* + S^*R \right\} + C + H \quad .$$

The coefficient of the $SR^* + S^*R$ term is approximately constant when $k_2 t|S|^2$ is sufficiently small.

The light output from the hologram is

$$A_{out} = A_{in} T_t \quad . \tag{48}$$

Letting the optical input to the hologram be the original subject beam amplitude function, then

$$A_{out} = S(x_2, y_2) T_t \quad . \tag{49}$$

Neglecting the constant and higher order terms (C + H) of equation (35), the optical output from the hologram is

$$A_{out} = k'(SR^* + S^*R)S \quad , \tag{50}$$

where

$$k' = T_0 \, k_2 t \exp\left\{i\left[k_2 t(S^2 + R^2) + \frac{\pi}{2}\right]\right\} - k_1 t \quad . \tag{51}$$

Therefore,

$$A_{out} = k'(SSR^* + S^*SR) \tag{52}$$

and, when the input is some modified subject beam $S'(x_2,y_2)$, the output becomes

$$A_{out} = k'(SR^* + S^*R)S' \tag{53}$$

$$= k'SS'R^* + k'S^*S'R \quad . \tag{54}$$

The term, k'S*S'R, is of principal interest since the optical correlation measurement will be obtained from it. The constant k' may be combined with the amplitude R_o of the function R since the reference beam is constant across the beam. One may consider the term k'S*S'R as a reconstruction of the reference beam modulated by the S*S' factor, where

$$S^*(x_2,y_2) = \mathfrak{F}^*[s(x_1,y_1)] \tag{55}$$

and

$$S'(x_2,y_2) = \mathfrak{F}[s'(x_1,y_1)] \quad . \tag{56}$$

It can be shown that the Fourier transform of the cross correlation of two functions is the product of the complex conjugate of the Fourier transform of one function and the Fourier transform of the other [15],

$$S^*(x_2,y_2)S'(x_2,y_2) = \mathcal{F}\left[\int\int_{-\infty}^{\infty} s^*(x_1,y_1)s'(x_1 + x_2,y_1 + y_2)dx_1dy_1\right] \quad . \tag{57}$$

Here, the symbol $\mathcal{F}(f)$ represents the Fourier transform of an arbitrary function, f, and the remaining factor on the right side of the equation is

$$\int\int_{-\infty}^{\infty} f_1{}^*(u,v)f_2(u + x, v + y)dudv \quad ,$$

whose format represents the cross correlation integral of the functions f_1 and f_2.

The cross correlation is obtained optically by taking the Fourier transform of the product $S^*(x_2,y_2)S'(x_2,y_2)$. It should be noted that the Fourier transform of a function yields the original function only through an inverse Fourier transformation. Only the Fourier transform may be achieved through a simple lensing system and not the inverse Fourier transform. Although no inverse transform may be obtained, the transform of a transform provides a useful result. A function f(x,y) may be transformed in two dimensions into $F(\alpha,\beta)$ which may be transformed into f(-x,-y) within a multiplicative constant, provided the transform lenses are of equal focal lengths [20]. The point of interest in the correlation plane is $x_3 = 0$, $y_3 = 0$. Therefore, the reversal of coordinate polarity is of no great consequence (Fig. 3).

The amplitude function in the correlation plane is related to the subject input plane as follows:

$$F(x_3,y_3) = \mathcal{F}\left\{\mathcal{F}\left[\int\int_{-\infty}^{\infty} s^*(x_1,y_1)s'(x_1 + x_2, y_1 + y_2)dx_1dy_1\right]\right\} \tag{58}$$

$$= \int\int_{-\infty}^{\infty} s^*(x_2,y_2)s'(x_2 - x_1, y_2 - y_1)dx_2dy_2 \quad , \tag{59}$$

where $F(x_3,y_3)$ is the correlation function. Detection of the intensity, $F(0,0)^2$, is obtained by locating the detector behind a pinhole centered at $x_3 = 0$, $y_3 = 0$. The measurement made is

$$\left| \iint_{-\infty}^{\infty} s^*(x_2,y_2)s_1(x_2,y_2)dx_2dy_2 \right|^2 \quad ,$$

which is the intensity of the optical correlation within a constant multiplier, K. The maximum correlation value is obtained when

$$s'(x_1,y_1) = s(x_1,y_1) \quad ; \tag{60}$$

this case is defined as autocorrelation. Normalizing the correlation function in equation (59), the constant, K, is defined by

$$K \iint_{\infty}^{\infty} |s(x_1,y_1)|^2 \, dx_1dy_1 \equiv 1 \quad . \tag{61}$$

Therefore, the normalized amplitude function is

$$F(0,0) = \frac{\iint_{\infty}^{\infty} s^*(x_2,y_2)s'(x_2,y_2)dx_2dy_2}{\iint_{\infty}^{\infty} |s(x,y_1)|^2 dx_1dy_1} \quad . \tag{62}$$

The measured value may be expressed as a fraction or as a percentage of autocorrelation.

E. Forces in Solder Joints

Solder joints on printed circuit boards are subject to forces during their storage and use. These forces may originate from dynamic loading, for example, vibration or static loading induced by changing temperature. Only the temperature related forces are

considered in this study. Printed circuit boards are constructed of materials possessing different coefficients of thermal expansion, which causes forces to exist in the materials when the temperature of the circuit board changes. The magnitude and direction of these forces and the results produced are analyzed in this section.

The most frequently used solder joints are the stud types shown in Figures 4a and 4b and the clinched type (i.e., the lead wire has been bent over and soldered) as shown in Figures 4c and 4d. Experiments were limited to these types of solder joints.

The configuration of a stud type joint is detailed in Figure 5. In the double-sided joint shown in the figure, the internal forces arise from temperature changes of the joint. Single-sided joints have forces imposed on them that originate external to the joint. The responses of the joints to forces originating in these two ways are considerably different. For an axial force imposed on the lead wire of a single-sided joint, the force may be considered independent of the response of the solder joint. A static force applied to this type of joint will immediately compress the circuit board and expand the lead wire. In addition to an immediate response of the solder, the joint will also exhibit a property called creep. Creep may be described as a process by which a material under stress will inelastically deform in a manner such as to reduce the stress.

Those forces that originate in a double-sided solder joint as the result of temperature changes are related primarily to the differences in the coefficients of thermal expansion of the circuit board material and of the lead wire that bridges the two sides of the board. The forces are proportional to the temperature change for slowly changing temperature, which is defined here as a rate of change of temperature sufficiently slow that the temperature gradients within the circuit board are small compared to the temperature change. A rate of 5°C per minute is typical for the testing of printed circuit boards in space flight hardware. Damage of electronic components tested in this manner does not include thermal shock damage.

The significant parameters employed in the calculation of forces in circuit boards are shown in Table 1 and Figure 5. Symmetry about a plane bisecting the circuit board parallel to its faces is assumed; also, no forces are assumed to be present within the solder joint at room temperature. The latter assumption is based on the creep characteristics of solder. For a change in temperature, each component part of the circuit board changes dimension according to the following formulation:

$$\delta = (\text{length})(\text{thermal coefficient of expansion})(\Delta T) \quad , \tag{63}$$

where ΔT is the change in temperature. Considering first the circuit board material of thermal coefficient of expansion, α_L, and a positive change in temperature, the change in dimension will be

$$\delta_L = L\alpha_L \Delta T \quad . \tag{64}$$

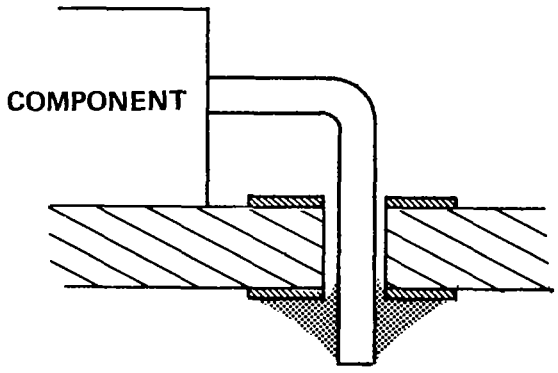

a. Stud mounted component.

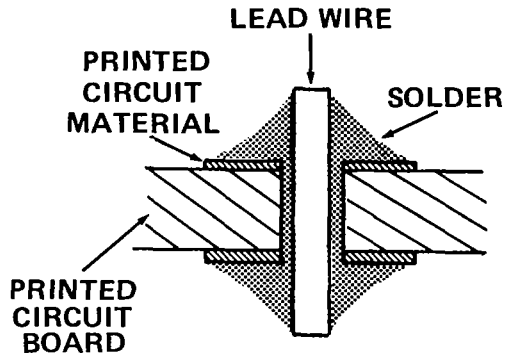

b. Stud feed-through.

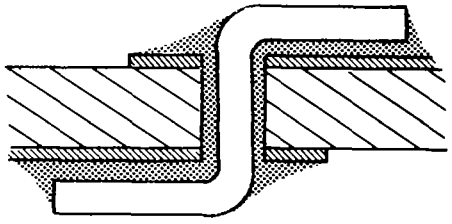

c. Clinched joint (cutaway).

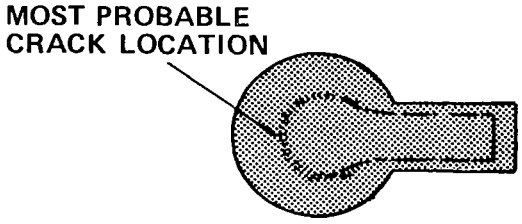

d. Clinched joint (top).

Figure 4. Typical printed circuit board solder joint connections.

For the same length of lead wire the change in wire length is

$$\delta_W = L\alpha_W \Delta T \quad . \tag{65}$$

The difference in these amounts of expansion is

$$(\delta_L - \delta_W) = L(\alpha_L - \alpha_W)\Delta T \tag{66}$$

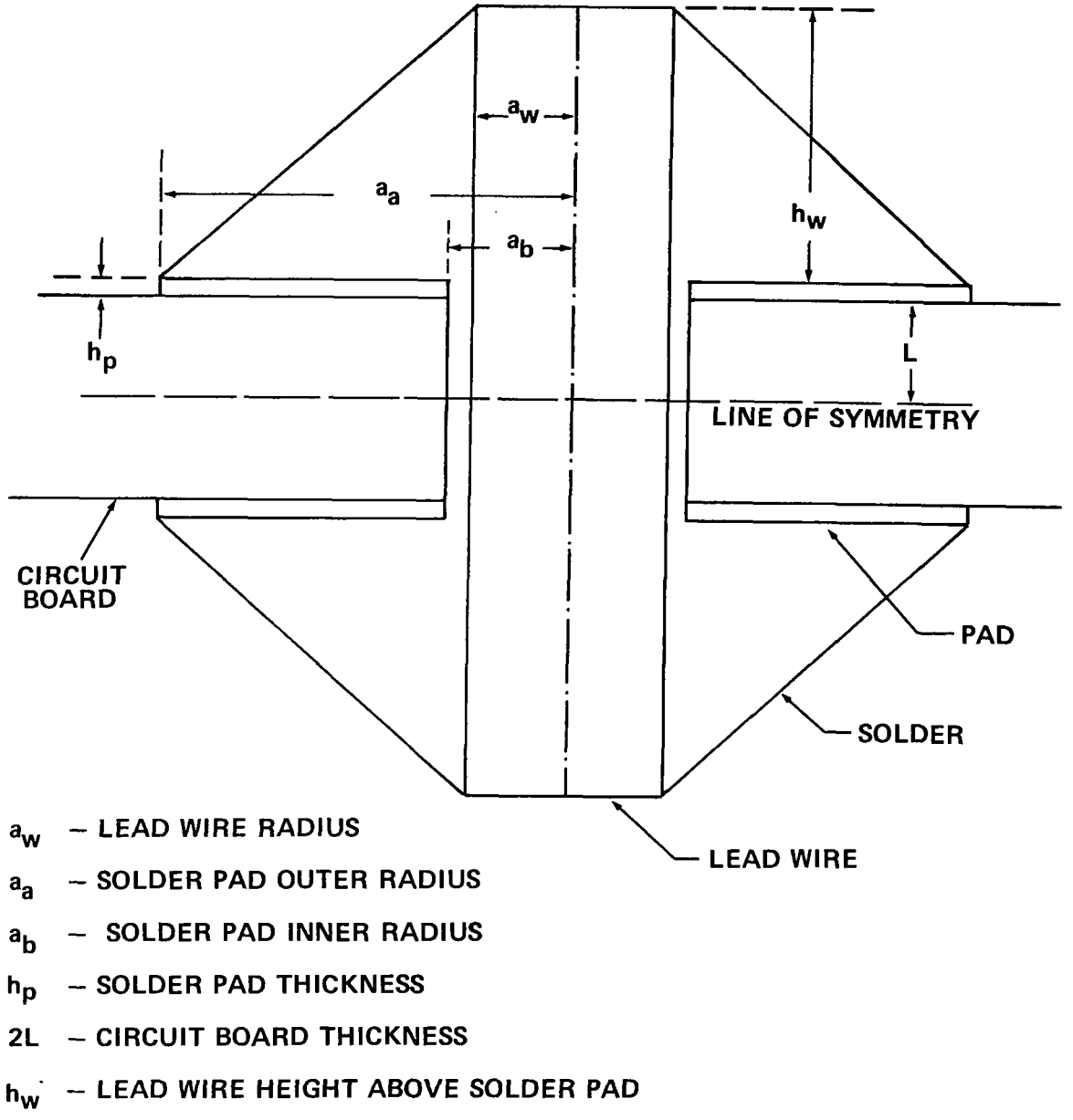

Figure 5. Detail of stud-type, feed-through solder joint.

with the circuit board material expanding the greater amount because of the particular types of materials used in this work. The dimensions of these two materials are constrained by the solder to remain equal in length. The induced force, F, needed to constrain the materials to remain equal in dimension may be calculated. These calculations neglect the effect of creep.

TABLE 1. PHYSICAL PARAMETERS OF MATERIALS IN PRINTED CIRCUIT BOARDS

α_w – Coefficient of expansion of wire
E_w – Modulus of elasticity of wire
σ_w – Tensile stress in wire
a_w – Radius of wire cross section
h_w – Height of wire above solder pad
L – Half thickness of circuit board material
α_L – Coefficient of expansion of circuit board material
E_L – Modulus of elasticity of circuit board material
σ_L – Tensile stress in circuit board material
h_p – Solder pad thickness
a_a – Solder pad outer radius
A_p – Solder pad area
a_b – Solder pad inner radius (hole radius)
A_w – Wire cross sectional area
ΔT – Change in temperature
τ – Shear stress

It is further assumed that the circuit board is compressed over the area of the solder pad. The lead wire supports a force of equal magnitude and opposite direction and is thereby stretched. The amount of compression of the circuit board semi-thickness, L, and extension of the lead wire lengths are, respectively,

$$\gamma_L = \frac{-FL}{E_L A_p} \tag{67}$$

and

$$\gamma_w = \frac{FL}{E_w A_w} \quad . \tag{68}$$

Here, γ_L and γ_w are the changes in circuit board and wire dimensions as a result of the induced force, E is the modulus of elasticity, and A_p and A_w are the solder pad and wire cross sectional areas, respectively. Also,

$$\delta_L - \delta_w = \gamma_w - \gamma_L \tag{69}$$

$$= \frac{FL}{E_w A_w} - \frac{-FL}{E_L A_p} \tag{70}$$

$$= L(\alpha_L - \alpha_w)\Delta T \quad . \tag{71}$$

Therefore,

$$L(\alpha_L - \alpha_w)\Delta T = FL \frac{1}{E_w A_w} + \frac{1}{E_L A_p} \quad , \tag{72}$$

where the force necessary to maintain equal dimensions of the printed circuit board and the lead wire is

$$F = \frac{(\alpha_L - \alpha_w)\Delta T}{\frac{1}{E_w A_w} + \frac{1}{W_L A_p}} \quad . \tag{73}$$

These forces compress the circuit board material and stretch the lead wire such that they maintain equal dimensions. These forces are equal and opposite in direction (Fig. 6a). These forces counterbalance each other by a shear stress at the interface between the lead wire and the bulk solder. This interface is a cylindrical volume external to the lead wire and produced by the dissolution of copper from the lead wire into the surrounding solder. The diameter of this interface is approximately equal to the solder pad dinner diameter ($2a_b$) and the height of the interface is equal to the height (h_w) of the lead wire above the solder pad. The shear stress is assumed to decrease linearly with height above the solder pad as shown in Figure 6b. The shear stress, τ, at any height, h, above the solder pad will be

$$\tau(h) = \tau_{max} \frac{h_w - h}{h_w} \quad , \tag{74}$$

where τ_{max} is the maximum shear stress at the inner circumference of the solder pad. The average shear stress is, therefore,

$$\tau_{aver} = \frac{\tau_{max}}{2} \quad , \tag{75}$$

and the total induced force is

$$F = \frac{\tau_{max}}{2} (2\pi a_b h_w) \tag{76}$$

$$= \pi a_b h_w \tau_{max} \tag{77}$$

or

$$\tau_{max} = \frac{F}{\pi a_b h_w} \tag{78}$$

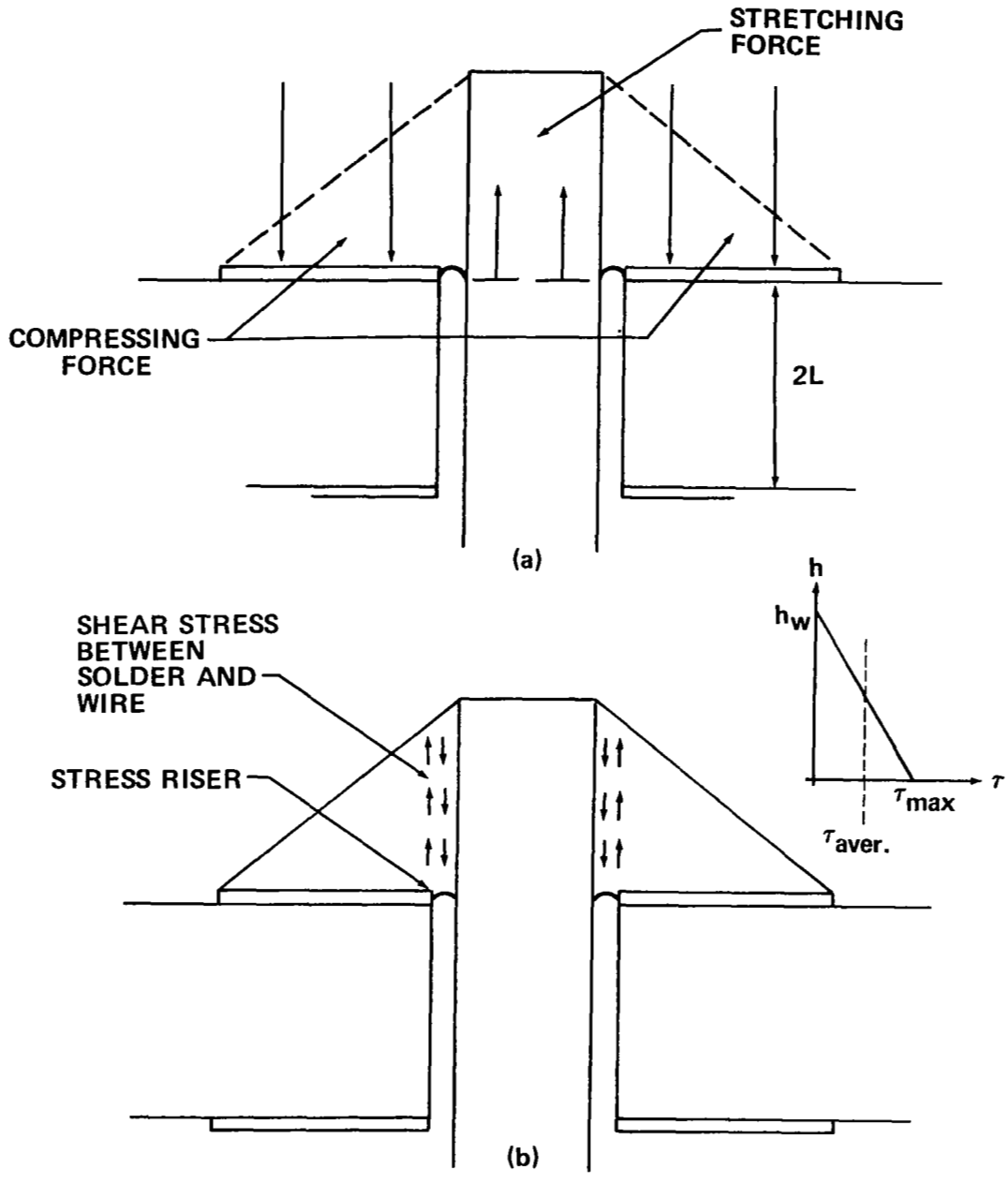

Figure 6. Forces in stud type solder joint.

The foregoing treatment is an approximation of the mechanism occurring in stud type solder joints. It should be recognized that several things affect the accuracy of that approximation. The geometrical configuration of a solder joint under stress is time

dependent because of creep. Therefore, the length of time transpired since a temperature change has occurred will determine the magnitude of internal forces. The magnitude of ambient temperature determines the rate at which creep occurs. The soldering temperature, the duration of heat application, and the rate at which cooling of the solder joint occurs all affect the quality of the solder joint. The solder increases its complexity by the dissolution of the materials being joined; this changes the characteristics of the solder and the solder junction. However, the simplified model described above established the basic force relationships.

IV. EQUIPMENT AND EXPERIMENTAL PROCEDURES

Experimental procedures were established for the determination of the relationships between a measurement of optical correlation, the forces involved in a printed circuit board solder joint, and the ability of the joint to survive, which will be designated as "survivability" throughout the remainder of this report. The feasibility and limitations of nondestructive testing of solder joints could be evaluated from these relationships. The effect of axial force applied to the lead wire of a circuit board solder joint on the life expectancy of the joint is known from the literature [5]. It has been demonstrated that life expectancy of solder joints depends upon the structural configuration of the joints [5]. The approach taken in the present work was to study the optical correlation measurements as they varied in response to forces induced into the solder joints. In addition, the relationship between optical correlation measurements and the type, shape, and internal structure of the solder joints was studied.

Forces within a solder joint normally originate from vibrations of the electronic package and temperature variations. Only the latter source is considered in this study. Changes in temperature induce forces in printed circuit boards as a result of differences in the coefficients of thermal expansion of the materials mounted on the board. Cyclic forces result from cyclic temperature changes. These forces cause a fatigue type degradation in the solder. Optical correlation measurements have been successfully used to predict the onset of fatigue failure in materials [11,13]. These experiments were destructive in nature. By contrast, the procedures reported here were nondestructive.

A series of tests was conducted to demonstrate how optical correlation measurements of solder joints on printed circuit boards are affected by forces in the joints and whether optical correlation measurements can be employed in revealing the tendency towards failure of solder joints. By the application of calibrated mechanical loads to solder joint lead wires, it was possible to determine the effect of known forces on optical correlation measurements. These tests provided the information necessary to establish the nondestructive thermal testing procedures. Nondestructive testing demonstrated the difference in response of different solder joints to equivalent thermally induced forces. The data from the thermal tests provided information which, when used in conjunction with the results from the destructive tests, could determine likelihood of survival of the solder joints.

In summary, the experimental results were obtained from three procedural steps: (1) optical correlation measurements versus mechanical force applied to the solder joint lead, (2) optical correlation measurements versus force induced into the solder joint by a change in temperature of the joint, (3) a destructive series of temperature cycles.

A. Optical Correlation Equipment

The optical arrangement (Fig. 7) employed in this work had the requirements typical of systems for optical correlation measurements. Mechanical stability to within 1/10 of the wavelength of incident light is required during exposure for holographic construction. This level of stability was maintained throughout the exposure time, which varied from 1/128 second to 2 seconds. The optical system was mounted on a 1.22 by 1.83 m granite table supported by air piston vibration isolation mounts. Massive supports were employed for optical components; the room temperature was stabilized to plus or minus 2°C. These precautions also were taken to assure long term mechanical stability and consistency of measurements. This degree of stability allowed measurements to be made over a period of several days employing a single hologram. However, normal procedures allowed measurements on a single hologram to be completed within 8 hours of the exposure of the hologram. Components (Table 2) were selected for mutual consistency of size. Ten centimeter clear aperture transform and correlation lenses, a 10 cm diameter collimator, and a 10 by 12.7 cm recording medium were employed. The optical axis was positioned 25.4 cm above the surface of the granite table.

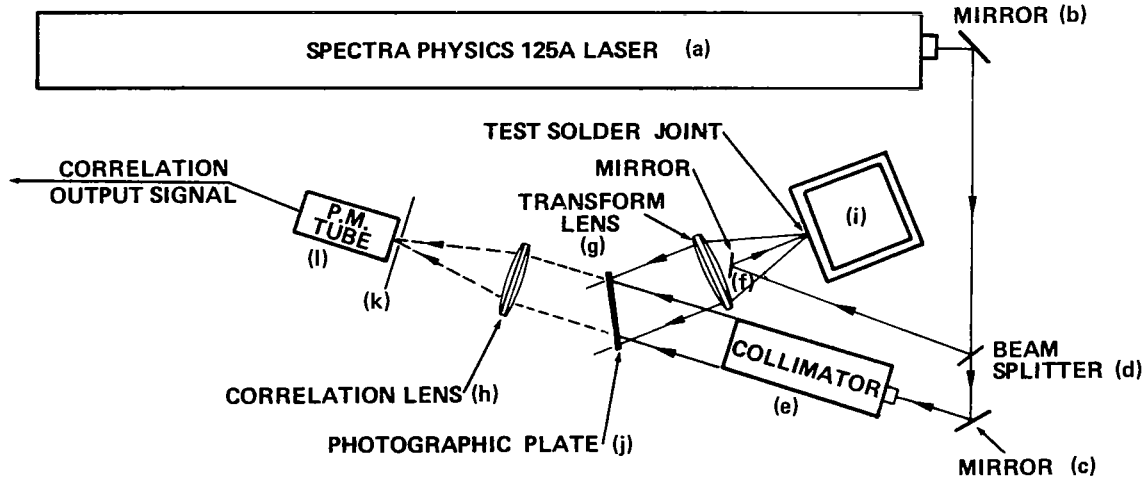

Figure 7. Optical correlation measurement system.

TABLE 2. OPTICAL CORRELATION SYSTEM OPTICAL COMPONENTS
(Refer to Fig. 7)

(a)	Laser – Spectra-Physics (Mountain View, California), Model 125A helium-neon continuous wave laser with a nominal output of 50 mW and a wavelength of 632.8 nm.
(b,c)	Mirrors – GCO Corporation (Ann Arbor, Michigan), front surface mirrors with adjustable height, rotation, and tilt.
(d)	Beam Splitter – Jodon Engineering Associates (Ann Arbor, Michigan), Model UBA-200 variable beam splitter.
(e)	Collimator – Tropel, Inc. (Fairport, New York), Model 280 laser collimator (100 mm exit aperture) mounted on a Weiser/Robodyne Corporation (Silver Spring, Maryland) precision elevation table.
(f)	Mirror – Approximately 5 mm diameter front surface mirror centered on the optical axis and mounted on the Fourier transform lens mount.
(g,h)	Lenses – Tropel (Fairport, New York), Model 1520-100, F/2.0, f-200 mm, MgF_2 coated for reflection of less than 1 percent and diffraction limited at 632.8 nm.
(i)	Solder Joint Mount – 20 cm by 20 cm by 27.5 cm mount of 1.9 cm thick steel stock.
(j)	Holographic Plate Holder – Jodon Engineering Associates (Ann Arbor, Michigan), Model MPH-45 x-y micropositionable plate holder for 10 cm by 12.5 cm plates, mounted on a Weiser/Robodyne Corporation (Silver Spring, Maryland) Model 149 two (horizontal) axis micropositionable mount.
(k)	Pinhole – 200 μm diameter pinhold provided with three axial adjustments.
(l)	Photomultiplier – Amperex Electronic Corporation (Hicksville, New York), 150 CVP tube in an Electro Optics Associates (Palo Alto, California) Model PM-101 housing and utilizing a 10 kΩ loading resistance. Normal cathode voltage of -1000 V.

Laser output variations could contribute to measurement error. The normal warmup time of 10 to 15 minutes was found to be inadequate. Power output variation was the principal laser contributor to measurement error. Therefore, it was necessary to monitor the power output to establish that the laser was operating at steady state. This measurement indicated that steady state operation was attained only after an hour or more of warmup. On this basis no holographic exposure or optical correlation measurement was made without proper warmup of the laser. In practice the laser was operated continuously to avoid long warmup times. The laser was turned off only when required for power rewiring or for similar purposes.

The Spectra-Physics Model 125A laser was employed because of its adequate output power, cw type output, high output stability, air cooling, and dc excitation. The output power requirement was established based on holographic efficiencies. The variation in the scattering properties of the surface of the solder made the laser output power requirements vary from one solder joint to another. However, the worst-case situation was satisfied by the laser employed. An exposure time of less than 2 seconds was necessary to meet the holographic recording stability requirement of the optical system. These requirements set a lower optical power limit to assure proper exposure of a 10 cm photographic plate.

The mirrors employed were front surface reflecting, high quality units with high reflectivity and low scattering characteristics. After initial alignment of the system, no additional adjustments of the mirrors were required. The small mirror (f) shown in Figures 7 and 8 was permanently attached to the transform lens mount. The mirror was permanently aligned during installation.

The reference beam path length was adjusted to be equal to the subject beam path length (within 1 cm) to minimize the effect of the relatively short coherence length of the laser output light. The minimum angle, θ, between the collimated reference beam and the subject beam was approximately 48°. The minimum beam angle was determined by the geometrical limitations imposed by the size of the mounted transform lens and the transform lens focal length (20 cm). The 10 cm diameter light beams intersected at the film plane 20 cm from the transform lens.

The transform lens affected the above beam intersection angle and the light gathering power, among other things. According to the formula,

$$\text{lines/millimeter} = 2 \sin(\theta/2)/\lambda \quad , \tag{79}$$

the spatial frequency generated when two light beams of wavelength λ interfere at an angle θ will be approximately 1220 lines per millimeter for λ 0f 632.8 nm and θ of 48°. This spatial frequency is well within the range of resolution of available photographic

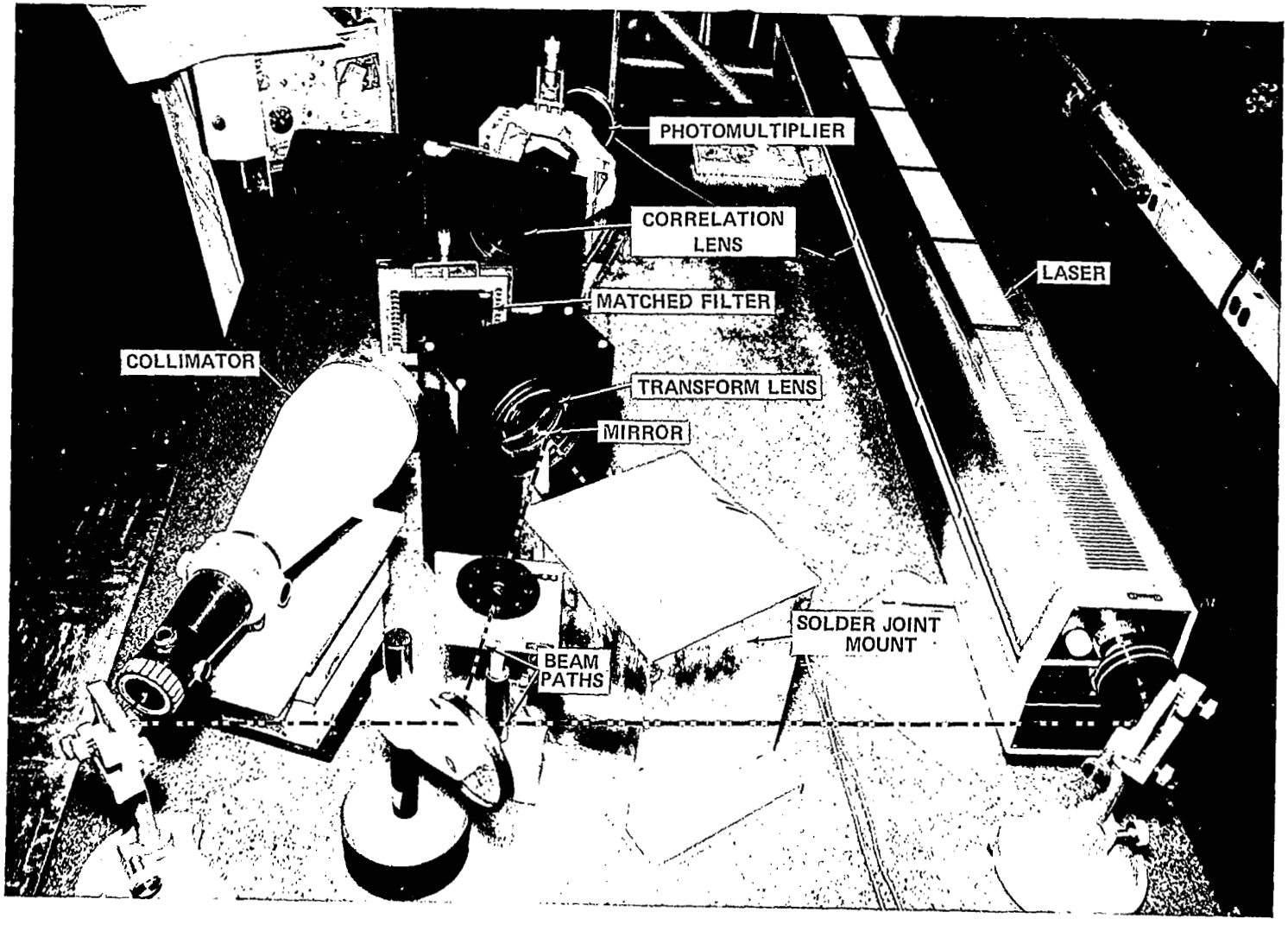

Figure 8. Photograph of optical correlation system – end view.

plates. The quality of the transform lens was determined by observing the diameter of the Airy disc formed by focusing collimated light. The Airy disc diameter was calculated to be 3.1 μm from the formula,

$$D_A = 2.44\lambda f/D \quad , \tag{80}$$

where D_A is the Airy disc diameter, f is the focal length of the lens, and D is the diameter of the incident light beam. A photographic exposure of the Airy disc indicated no major aberrations for monochromatic light, since the diameter of the developed spot was of the order of magnitude of the calculated Airy disc diameter.

The primary recording medium requirements for this application were adequate spatial resolution and a sensitivity commensurate with the exposure times permitted by the laser power and system vibration conditions. These requirements and the proper wavelength sensitivity were met by HR145P plates manufactured by GCO Incorporated. The 1300 lines or less per millimeter requirement imposed by the 48° reference-subject beam angle was within the 2000 lines per millimeter specification of the plates. An exposure of 10×10^{-7} to 40×10^{-7} J cm^{-2} (10 to 40 ergs cm^{-2}) at 632.8 nm is required for illuminating the plates. This amount of illumination is normally available in the optical system employed.

The procedure for processing the holographic plates (Table 3) was a standard procedure modified to produce optimum results. The resulting procedure satisfied the holographic efficiency, stability, reproducibility, and ease of development requirements. Nonuniformity of plate illumination caused by nonuniform scattering from the solder joint and nonuniform reference beam intensity made compromises necessary. For example, precise exposure and fixed reference-to-subject beam ratios were not possible. The illumination decreased radially from the center of the hologram in both reference-to-subject beam ratio and in exposure. The reference beam intensity varied by a factor of 5:1 from the center to the edge of the 10 cm diameter beam. The radial variation corresponded approximately to the decrease in intensity of the subject beam from the center to the edge. The radial variation of the optical intensity of the subject beam was a complex function of the subject surface and its scattering characteristics. As a result, the holograms were overexposed at the center and underexposed near the edges; also the beam balance ratio was too high in the center and too low near the edges. However, the resulting overall efficiency of the hologram proved adequate.

The density to which the plates were developed was individually determined for each plate. The HR145P photograhic plates have a peaked spectral sensitivity at 632.8 nm, permitting the use of a green darkroom light for observing the density of the plates during the development process. This visual inspection process for determining the final density of the plate produces a holographic filter in which both the overexposed center and the underexposed edges are relatively efficient.

TABLE 3. DEVELOPING PROCEDURE FOR VANDER LUGT FILTERS

Step 1.	Presoak hologram in water for 2 minutes.
Step 2.	Develop in Kodak D-19 developer for 2 to 5 minutes (nominally 4 minutes). Developing time is determined by visual observation using a 15 W green safe light and developing until a density of approximately 0.5 to 0.7 is estimated for the center of the hologram.
Step 3.	Soak for 30 seconds in Kodak Indicator Stop Bath.
Step 4.	Fix in Kodak Rapid Fix for 3 minutes.
Step 5.	Wash in running water for 10 minutes.
Step 6.	Soak in Pakosol for 30 to 40 minutes.
Step 7.	Allow 30 minutes of air drying before taking data.
Note 1:	All solutions at the temperature of 20° to 22°C. Dark condition is required from Step 1 through Step 4.
Note 2:	Step 5 is the final step in the normal holographic development procedure.

The holographic reconstruction efficiency, however, depended not only on density variation but also on phase variation. The holographic efficiency could be improved by employing Pakosol (a product normally utilized for generating flat photographic prints and manufactured by Pako Corporation, Minneapolis, Minnesota) as a final soak. A hologram removed from the final water wash and immediately installed in the optical system has an efficiency that decreases as it dries. The final efficiency is only a fraction of the initial efficiency. However, the holograms treated in Pakosol maintain an approximately equal efficiency through the drying process. The effect of the Pakosol treatment increases the efficiency and stability with duration of the Pakosol soak. No further significant improvements are obtained by extending the soak for more than 45 minutes. Efficiencies of holograms soaked in Pakosol were higher than the theoretical efficiency of a purely amplitude attenuation hologram; therefore, a phase attenuation component must be present in the recorded function. It is not known whether the phase component resulted from an index of refraction change with exposure variation or from physical relief induced into the emulsion by selective shrinkage of the gelatin. However, the high spatial frequency attained with the hologram recorded with a beam angle of 48° would preclude major surface relief contributions to the reconstruction efficiency [17].

The 10 cm diameter collimator provided an optimum compromise between uniformity of output intensity and total output power. This compromise was implemented by employing a pinhole spatial filter which truncated only the periphery of the beam. The compromise provided for less optical power loss in the collimator.

Adjustments to the system could be classified into two categories: adjustments made prior to system operation and adjustments normally made during the operation of the system. Those adjustments made prior to operation of the system were alignment adjustments and consisted of system component placements and screw adjustments. Component positions were dictated by such requirements as equal optical distances for reference and subject beams, constant 25 cm optical axis distance above table height for all light beams, and perpendicularity of lenses to the beams. A fine adjustment of the correlation plane pinhole was necessary to center it on the light spot produced by the reference beam as it was focused by the correlation lens. It is interesting to note that the correlation spot produced by the reconstructed reference beam did not coincide with the original pinhole position. This lateral shift was shown by Douklias and Shamir [21] to be related to emulsion changes that occur during photographic processing of the filter.

Those adjustments made during the operation of the system were primarily filter adjustments. An x-y adjustable filter holder was mounted on a y-z translating base (Fig. 9). The plate holder was designed in a manner to allow its precise relocation in the optical system. The photographic processing of the plate slightly modified the position and spacing of the interference fringes of the filter as a result of changes in the photographic emulsion. However, the adjustments needed to compensate for these changes were small and in some instances not required.

B. Electrical Equipment

Associated with the optical system employed in this work was electrical and electronic equipment (Table 4 and Fig. 10) designed to monitor and control the system and to produce and record the inputs and outputs required for analysis of the test results.

The laser light output was controlled by an automatic electronic shutter. Exposure times of less than 0.01 second to several seconds could be established by a discrete time interval setting plus a variable multiplier. The shutter remained open for optical correlation measurements.

The output signals produced by the test system were temperature and optical correlation readings. The optical correlation signal resulted in a negative voltage, relative to system ground, from a photomultiplier. This voltage was proportional to the intensity of the two dimensional correlation integral amplitude function. This voltage output was provided simultaneously to the two oscilloscopes, a digital voltmeter and the strip chart recorder. The strip chart recorder was disconnected during mechanical testing. One

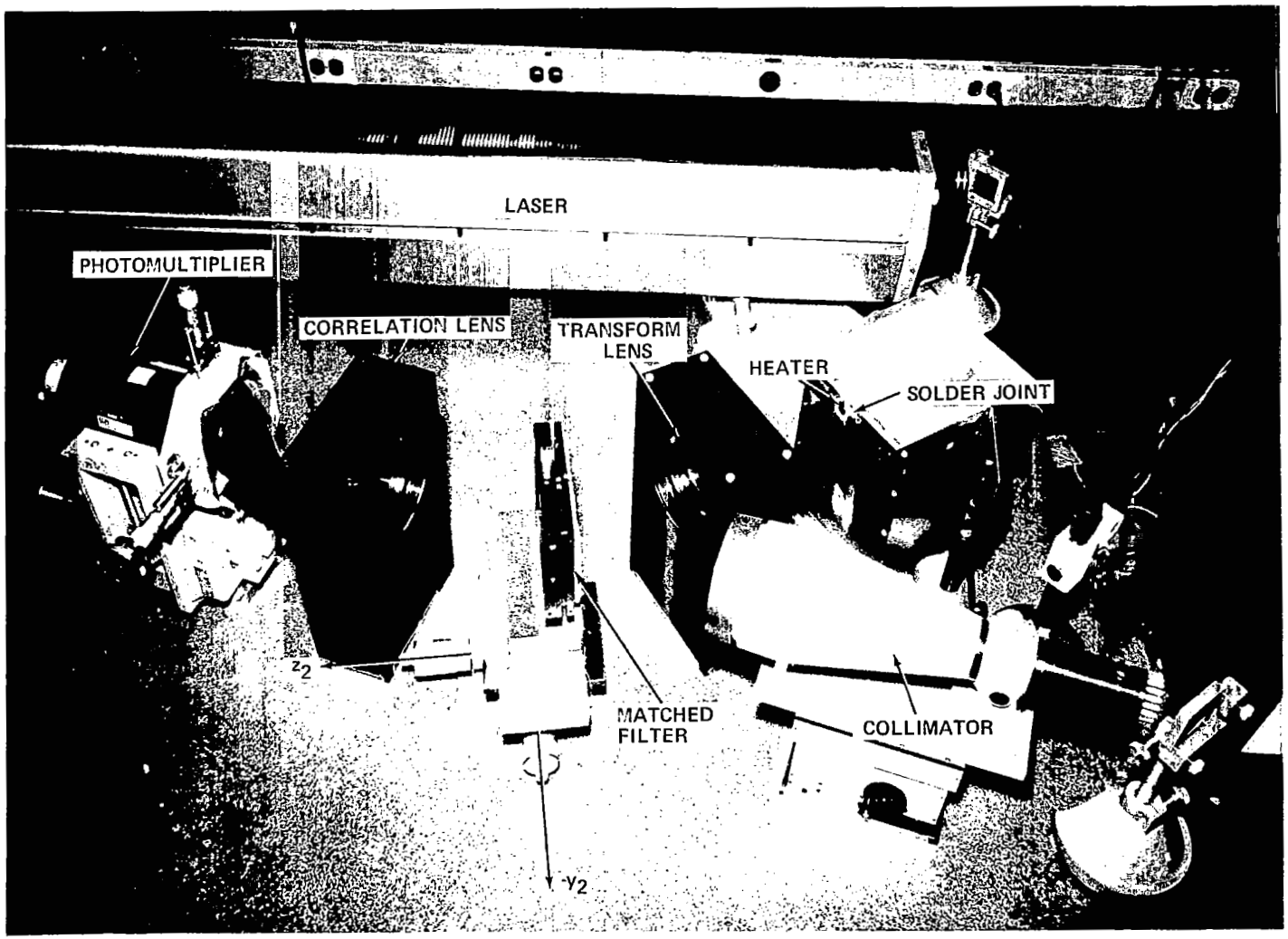

Figure 9. Photograph of optical correlation system – side view.

TABLE 4. OPTICAL CORRELATION SYSTEM ELECTRICAL AND ELECTRONIC COMPONENTS

(a) Electronic Shutter, Model ES-100, Jodon Engineering Associates (Ann Arbor, Michigan).
(b) Digital Voltmeter, Model 2460 A, United Detector Technology (Santa Monica, California).
(c) Digital Voltmeter, Model 2460 B, Hewlett-Packard Company (Palo Alto, California).
(d) High Voltage Power Supply, Model 242, Keithley Instruments, Inc. (Cleveland, Ohio).
(e) Heat Sensitive Strip Chart Recorder, 7700 Series, Hewlett-Packard Company (Palo Alto, California).
(f) Oscilloscope, Type 561 A, Tektronix, Incorporated (Beaverton, Oregon).
(g) Oscilloscope, Type R 454, Tektronix, Incorporated (Beaverton, Oregon).
(h) Power Supply, Model LM 234, Lambda Electronics Corporation (Melville, New York).
(i) Gray Lab Electric Timer, Model 300, Gray Company (Dayton, Ohio).

oscilloscope was set for a sweep time of several seconds to properly monitor short term correlation signal transients. The other oscilloscope was set for a sweep time of several microseconds to monitor average noise levels on the correlation signal. The recorder was employed to monitor the optical correlation system stability and to measure the optical correlation signal change induced by the thermal testing of the solder joint.

A digital voltmeter provided a digital output presentation of the optical correlation signal. This output varied from hundreds of microvolts to tens of volts depending upon the amount of light incident upon the photomultiplier. The digital voltmeter had the advantages of accuracy and a large dynamic range. In addition, this particular model of voltmeter integrated over a 1/10 second interval averaged out the 60 Hz line noise. This filtering process reduced the noise level to less than 10 μV. For normal signal values of 10 mV to 10 V, the electrical signal-to-noise level was at least 1000:1.

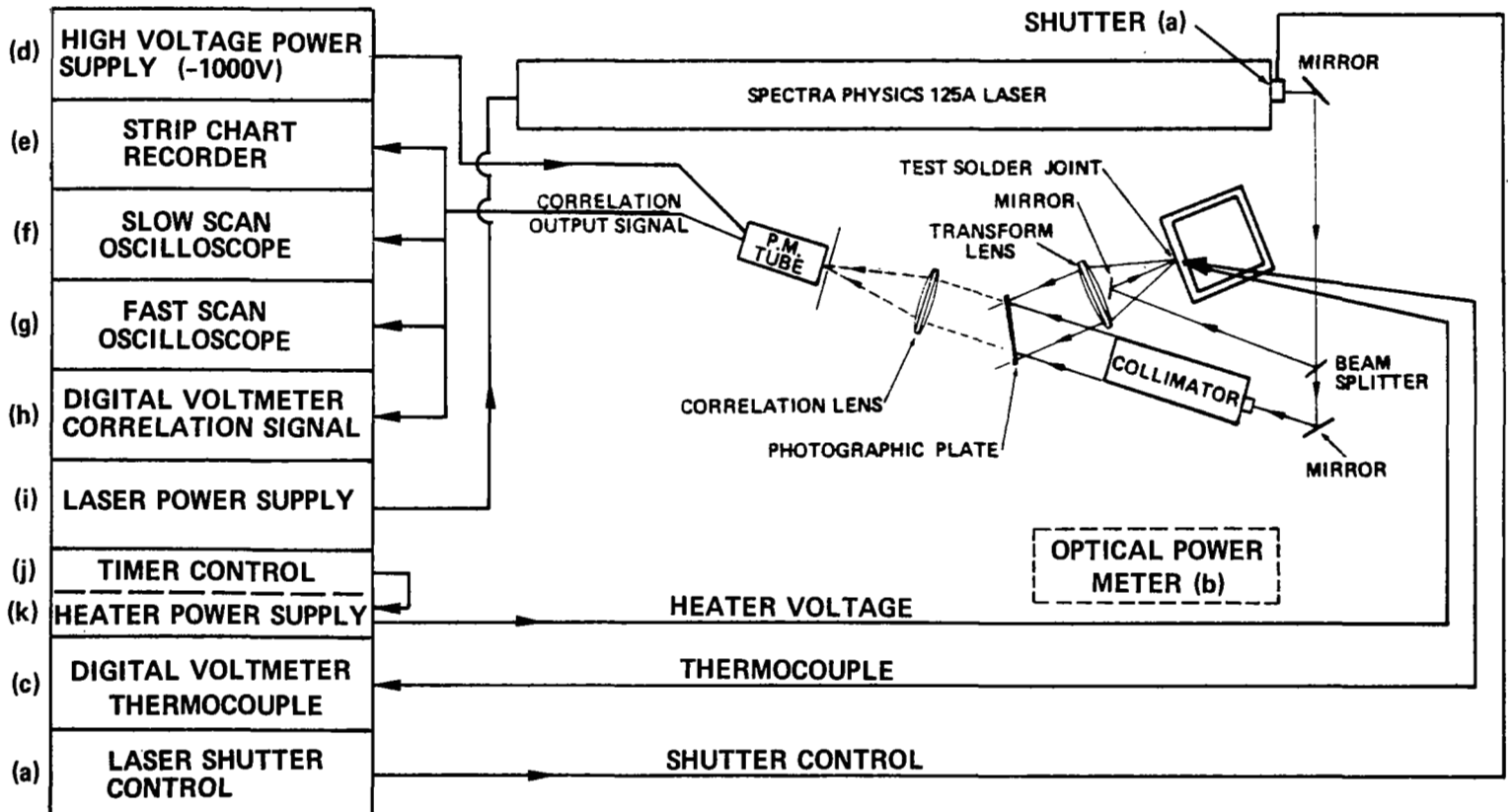

Figure 10. Electrical equipment associated with optical correlation measurement system.

Sensing of the solder joint temperatures was provided by iron-constantan thermocouples. The signals generated by the thermocouples were monitored by a digital voltmeter of the type used for measuring the correlation signal. Where needed, these temperature data were recorded concurrently with the optical correlation data. Accuracy of the thermocouple voltage reading corresponded to a temperature error of no more than 0.1°C. Details of the temperature measurements are discussed in Section IV.D.

The heating of the solder joint in the thermal phase of testing was accomplished with a fixed heater voltage and a fixed heating time. Heat was applied for 10 minutes in all thermal tests after preliminary testing had established the amount of heating required and the thermal time constants involved in the solder joint/heating element system (this procedure is detailed in Section IV.D). The electrical power to heat the solder joint was switched on manually and automatically switched off by a simple timer controlled power supply after 10 minutes duration.

The reference and subject beam intensities were measured employing a digital type power meter with a resolution of three digits and a sensitivity of 0.1 $\mu W/cm^2$. This power meter was also employed in measuring the laser output power to determine steady state laser operation.

C. Mechanical Testing Procedure

The mechanical tests performed in this work were directed toward establishing the behavior of solder joints, as observed through optical correlation measurements, while subjected to controlled and well defined forces. The requirements of accurately incrementing the test force levels were of prime importance in this procedure. Beginning with a procedure employed by an earlier investigator [14], the mechanical testing apparatus was refined to the test fixture illustrated in Figure 9.

In initial tests, strain was induced into the solder joint-lead wire assembly by mechanically elongating the lead wire. These tests duplicated previously made optical correlation versus strain measurements, and served to compare this optical system with an earlier system [14]. These strain tests accurately simulated the effects of temperature on solder joints. The creep characteristic of solder allows for relief of the force causing the deformation [22]. In subsequent mechanical tests the force induced in the joint was maintained at a constant level independent of the creep of the solder.

Following the strain tests, force tests were made utilizing a spring. A micrometer was employed to accurately and repeatedly elongate the spring, thereby producing a known force on the solder joint lead wire. The device was capable of producing a maximum force of 22.2 N and could be varied in increments of approximately 4.45×10^{-2} N. Lifetime tests on solder joints have been made at the Marshall Space Flight Center in which forces of this magnitude have eeen employed, and these provided at least

a qualitative basis for data comparison. These data were in the form of the lifetime of a solder joint versus dead weight suspended from the lead wire. These data indicated the maximum level of survivability and indicated a time dependence (creep) in the behavior of solder.

The major sequence of mechanical tests incorporated the device illustrated in Figure 11. Dead weight provided a constant force on the solder joint lead wire via a pulley arrangement. The pulley was supported by and rotated on ball bearings. The error produced by bearing resistance was no greater than 0.015 N. The dead weight container and connecting wires were made of fine gauge stainless steel. Masses that provided force on the lead wire were made in 22.7 and 45 g sizes. The error in these masses was of the order of 0.4 g and contributed a negligible error to the measurements.

The range of forces to which the solder joints were tested depended upon the type of solder joint under test. The mechanical tests were made on sample printed circuit boards as illustrated in Figure 12a. Construction of the test samples of solder joints varied in two aspects. In half the samples tested the lead wires were crimped against the printed circuit material and soldered (Fig. 12b), while the other half were the stud type (Fig. 12c). Of each of these groups, half of the group possessed plated-through holes while the other half possessed non-plated-through holes. Therefore, four distinct types of solder joints were tested by the application of static, constant force to the lead wire of the joints. These were identified as types A, B, E, and F as defined in Figure 12 and Table 5. The maximum force applied in these tests varied in magnitude from 1.09 N for some joints up to 6.88 N for others depending on the type of joint and its response.

The test procedure was repeated for all the test samples in order of their assigned identification number. Each sample was attached to the mounting bracket as shown in Figure 11. This procedure included the mounting of the printed circuit board to a plane surface of the mounting fixture with screws and attaching the lead wire to the empty weight container as shown in the figure. Particular care was taken at this point not to apply any force to the lead wire. This care was necessary since application of a force could slightly deform the solder in the joint and a long period of time would be required for equilibration.

After the optical correlation system had been prepared for mechanical testing, 15 minutes were allowed for all temperature gradients in the optical and mechanical components to subside before the holographic filter was constructed. After the laboratory was darkened and the holographic plate installed, a 3 minute delay was taken in which no movement was made in the room. This delay allowed time for the film plate and holder temperature to equilibrate and for vibrations in the optical table and equipment to subside. A remotely operated shutter then allowed illumination of the solder joint for a preset duration to properly expose the photographic plate.

After the photographic plate was developed and dried to form the holographic filter, it was reinstalled in the optical system. Any adjustments of the filter or pinhole

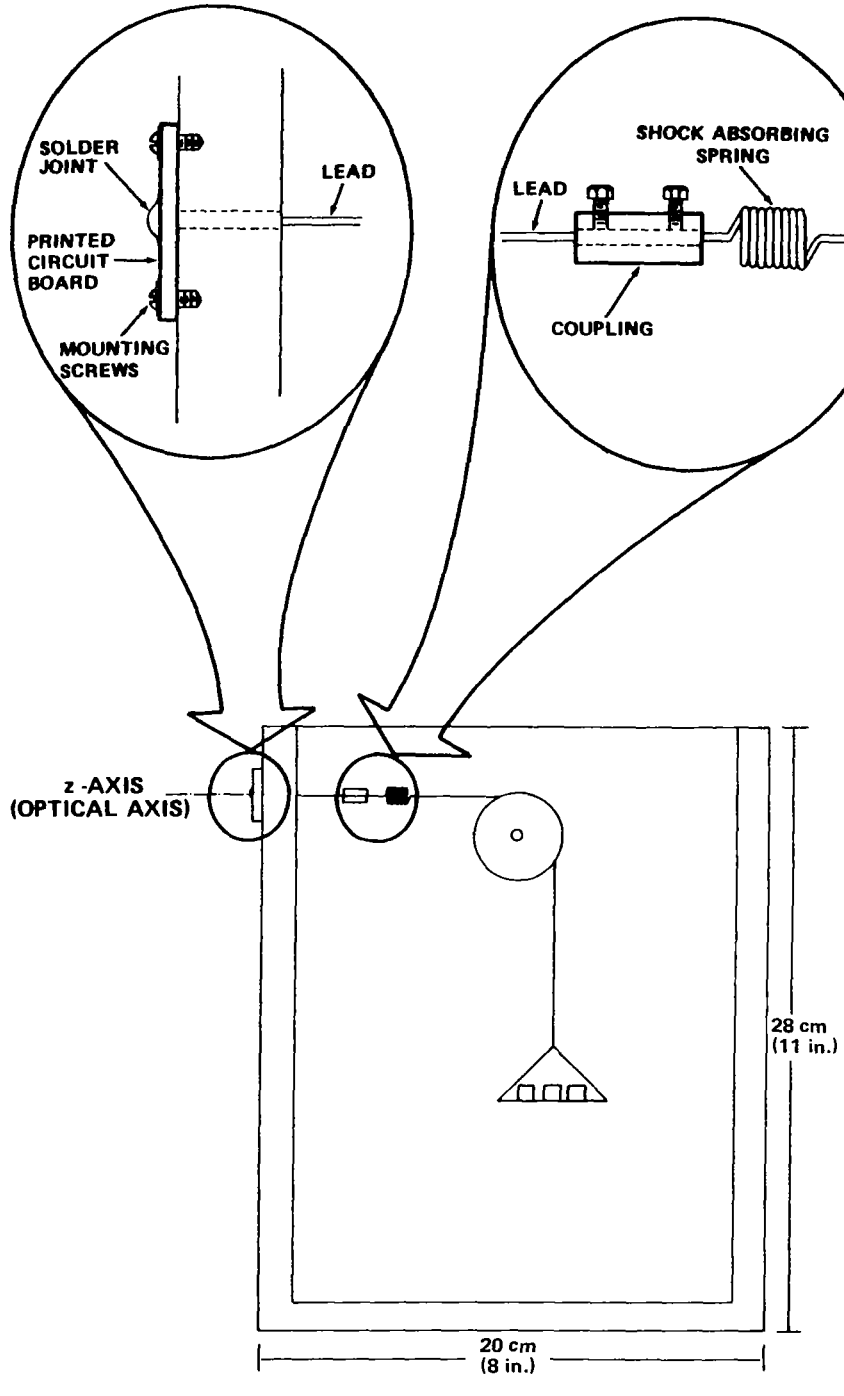

Figure 11. Mechanical tensioning device.

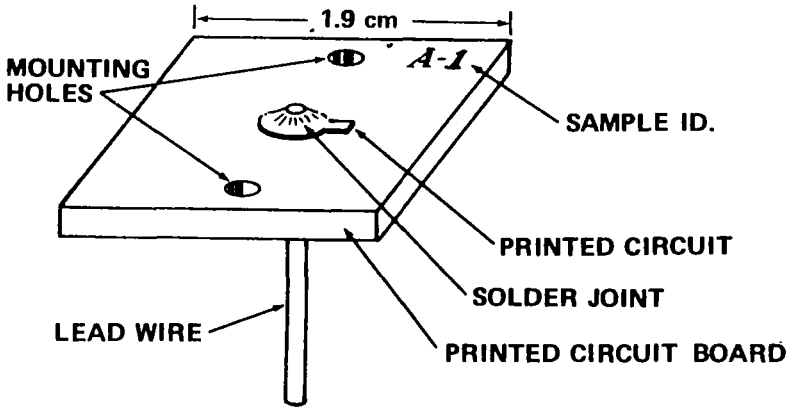

a. Sample circuit board with stud type solder joint.

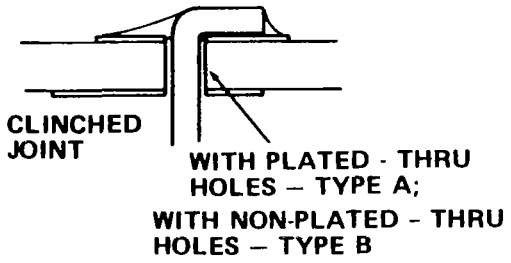

b. Clinched type solder joint.

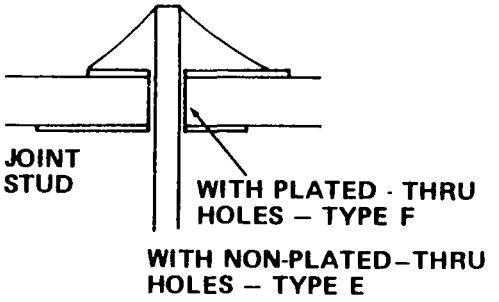

c. Stud type solder joint.

Figure 12. Solder joint types used in mechanical testing.

positions necessary to maximize the optical correlation signal were made at this time. The maximized signal was designated 100 percent optical correlation. In practice this designation was not precisely correct, because initial addition of force on the solder joint lead wire occasionally produced a slight increase in the correlation signal. This effect may be explained in terms of temperature changes resulting from laser heating of the solder joint and will be considered in detail in the section on thermal testing.

Beginning with zero force, incremental values of 0.227 N were added to the lead wire of the solder joint under test. After each increase in force, adjustments of the filter position in three axes and of the pinhole in two axes (Fig. 3) were made. The criterion for proper adjustment was a maximized optical correlation signal. An oscilloscope provided a continuous presentation of the correlation signal for adjustment purposes.

TABLE 5. TYPES OF SOLDER JOINTS TESTED

Type	Test	Solder Joint Characteristics
A	Mechanical	Plated-through holes
B	Mechanical	Non-plated-through holes
C	Thermal	Plated-through holes
D	Thermal	Non-plated-through holes
E	Mechanical	Non-plated-through holes
F	Mechanical	Plated-through holes
I	Thermal	Plated-through holes
II	Thermal	Non-plated-through holes

Following adjustments, a digital voltmeter provided the time averaged value. This value was recorded and used for data analysis. The values of applied force and correlation signal were recorded after each increase in applied force. An average of 1/2 to 1 minute was required to make adjustments and record data for each step increase in force.

The maximum force applied in the testing of each solder joint was that required to reduce the optical correlation signal to the order of 60 to 65 percent of the maximum signal. This limit was established through preliminary mechanical testing. A solder joint was permanently deformed if the force applied to the lead wire was in excess of that required to reduce the optical correlation signal below 60 percent. When permanent deformation occurred, the correlation signal did not return to 100 percent when the force was removed. Testing was terminated and another sample was installed in the system when the correlation signal had decreased to 60 percent. Preliminary tests, however, showed that a stepwise reduction in the lead wire force produced data approximately equal to that obtained during the stepwise increase in force.

A spring isolated the joint from any impulse that might occur as weights were added to the tensioning device (Fig. 11). The correlation signal quickly attained a reduced level after each weight was added. After each weight addition, the adjustments of filter and pinhole position were again made. The force applied to the solder joint lead wire not only deformed the solder joint but also compressed the printed circuit board. This compression displaced the test subject along the optical axis (Fig. 11). The filter position was adjusted in three dimensions to minimize the displacement effect. Pinhole repositioning in the (x_3,y_3) plane was required to compensate for a change in filter position.

D. Thermal Testing Procedure

The thermal testing of solder joints by which the optical correlation signal as a function of temperature change was observed was basic to the total experimental procedure involved in this research. Changes in the solder joint as a result of heating were caused by a slow temperature change and not by thermal shock. The testing procedure was designed to achieve a rate of temperature change sufficiently low that crazing of the solder and other thermal shock effects were avoided. The desired rate of temperature change was accomplished with a low wattage heating element of appropriate thermal mass and adequately separated from the test sample. The 6.4 W heating element (Fig. 13) consisted of five 2 Ω, 5 W resistors in series supplied with 8 Vdc. The configuration and location of the heating element generated a thermal radiation field such that temperature gradients about the solder joint and printed circuit board were small compared to the total change of temperature during testing.

The types of solder joints thermally tested are shown in Figure 14 and listed in Table 5. As with the mechanical tests, four types of solder joints were tested. Half of these were clinched and the other half were stud type joints. Each of the groups contained equal numbers of plated-through hole and non-plated-through hole types.

The characteristics of the heating element and the heated component were determined prior to taking thermal test data. The differential temperature between the center and the edges of the sample printed circuit board was measured and found to be approximately 1°C. Similar measurements determined that the thermal gradient from the heated front side of the board to the unheated back side was less than 1°C for this amount of heating. The average temperature in the solder joint and the printed circuit board increased approximately 10°C within 10 minutes after the heating element was turned on.

During the thermal testing, a thermocouple was attached to the circuit board to monitor the degree and rate of solder joint heating. The temperature monitoring system was calibrated by testing several printed circuit board samples. A temperature compensated voltage source replaced the 0°C reference thermocouple junction normally used. The thermocouple was then attached to the solder joint to measure the temperature of the joint. All temperature measurements were terminated after it was found that equal input power increased the temperature of each solder joint tested equally. This fact was checked for the last few thermally tested solder joints to verify that the heating element performance had not changed during the series of tests.

The heating level of 6.4 W, resulting from an 8 V heater excitation, was employed for all thermal testing. This level was based on its effect on the optical correlation measurements as determined in preliminary thermal testing. A 6 V heater excitation had the effect of changing the optical correlation signal by only a few percent. This small change in signal did not differ significantly from one test sample to another and thus did

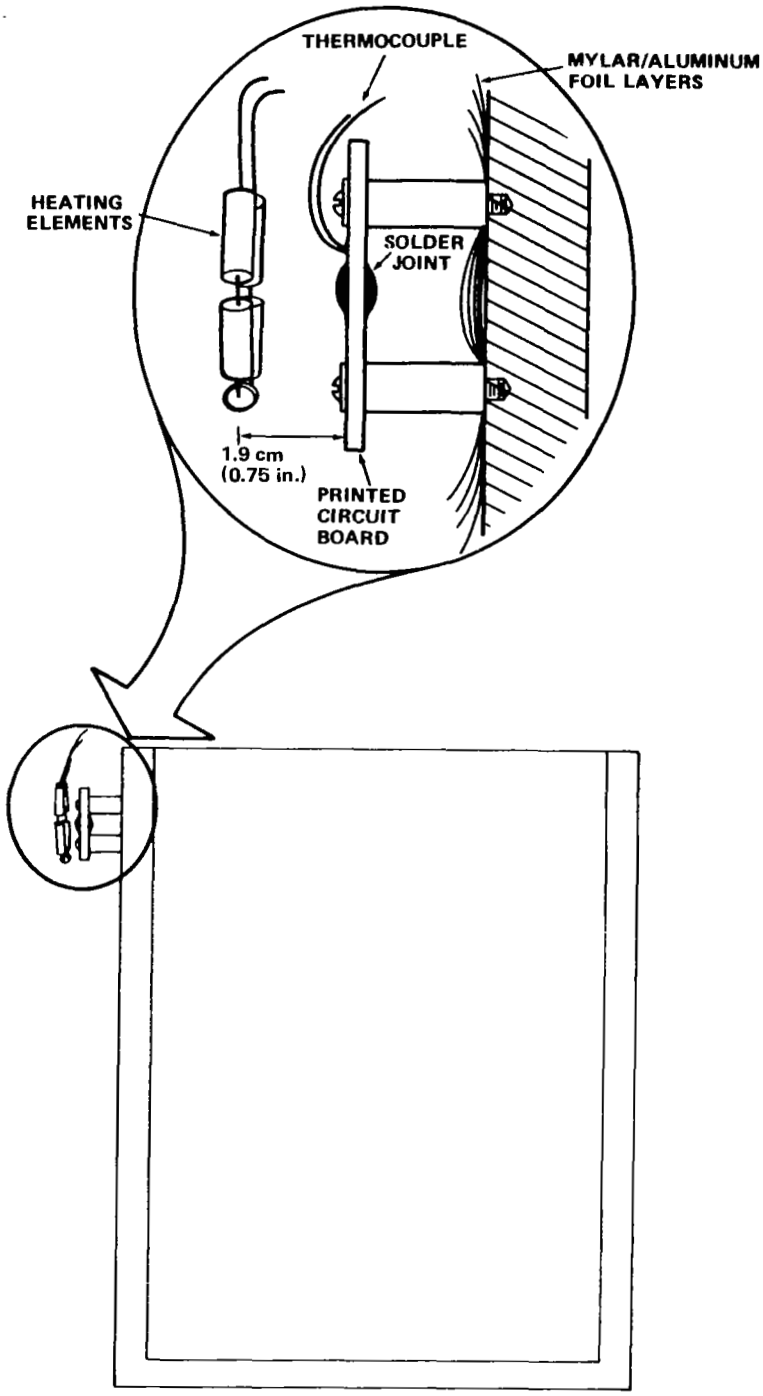

Figure 13. Thermal testing device.

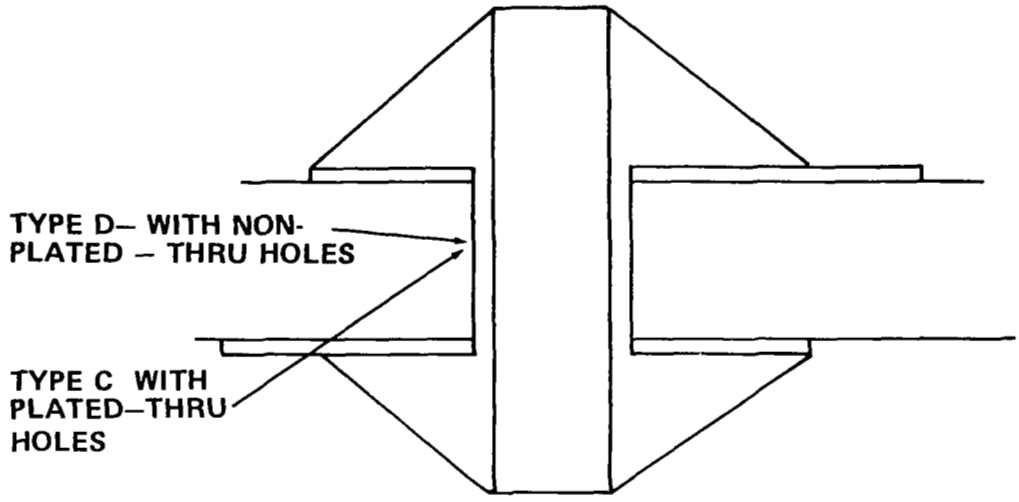

a. Stud type solder joint.

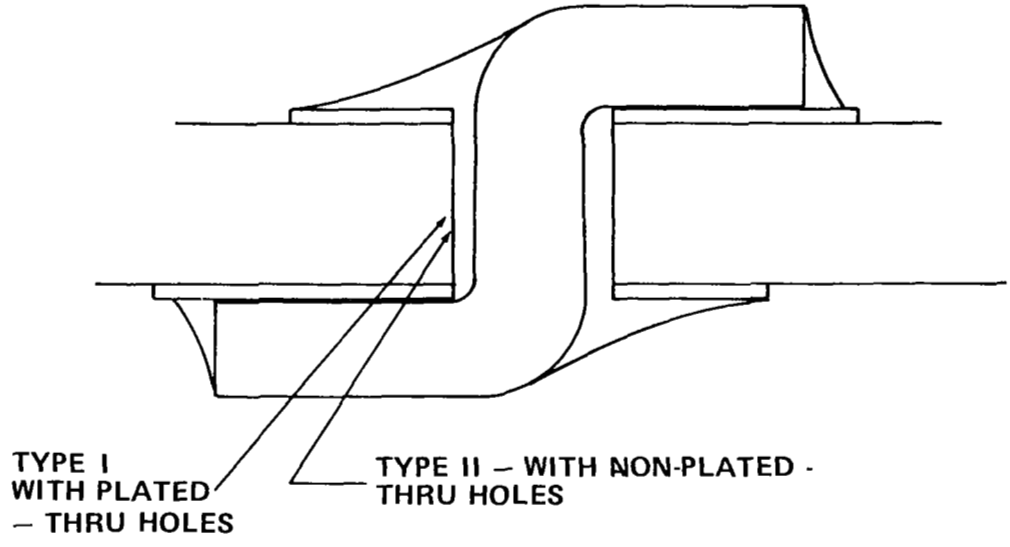

b. Clinched type solder joint.

Figure 14. Solder joint types used in thermal testing.

not adequately differentiate between samples based on their responsiveness to change in temperature. In contrast, heating resulting from a 10 V heater excitation reduced the optical correlation signal drastically for most samples. Heater excitation of 8 V was chosen since it provided an average loss of correlation signal of approximately 40 percent with a range of 3 to 80 percent.

A test to verify the repeatability of the matched filter system as applied in this work was included in the thermal test procedure. Two holograms were constructed for each of several solder joints to test the repeatability of the thermal test data from one hologram to the next. These holograms were exposed and developed in the same manner and were both, in turn, replaced in the optical system. The result was that the loss in optical correlation during heating of a solder joint was repeatable to within a few percent for most solder joints. This degree of repeatability was adequate.

A 10 minute heating cycle was employed to test the effect of heat on the solder joints. Then, the optical correlation of the solder joint was monitored for 10 minutes after removing the heater excitation. During the 10 minute heating cycle, the optical correlation decreased (approximately exponentially) with a thermal time constant of 2 minutes. A heating time of 5 thermal time constants allowed time for essentially stable correlation of the signal output. The strip chart data recording of the optical correlation signal was evaluated by visually noise averaging to provide the average correlation signal after 10 minutes of heating.

The solder joint test samples employed in the thermal testing had the same type of solder joint on both sides (Fig. 14). The test samples were tested first on one side, then on the reverse side.

It is noteworthy that the procedure for heat testing solder joints differed significantly from the mechanical testing procedure. This difference was that no maximization of optical correlation signal through system adjustments was undertaken after heat was applied to the test sample. Only internal forces are involved in the changes within the heated solder joint; no net displacement of the joint occurs in the tests. This difference in test procedure precludes easy comparison of the data obtained from the two tests.

E. Destructive Testing Procedure

Destructive tests were performed upon those solder joints that had been subjected previously to nondestructive thermal testing. These solder joints experienced a single temperature cycle from room temperature to 10°C above and back to room temperature during the nondestructive thermal tests. The destructive tests of the joints consisted of 190 cycles of temperature variations in which changes of 155°C occurred. The data from these two tests were then compared. The analysis of these data indicated to what extent optical correlation measurements could be employed in predicting the survivability of solder joints.

The test facility employed in the destructive testing of the solder joints was a controlled environmental chamber. This facility was programmed to control the chamber air temperature according to a controller cam. The cam rotated once each 2 hours

producing an air temperature profile with a 2 hour cycle. The air was continuously circulated by a fan to produce a uniform air temperature. The facility was turned on and off manually. The solder joint test samples were suspended within the chamber. The mounting configuration for the simultaneous destructive thermal testing of solder joints is shown in Figure 15.

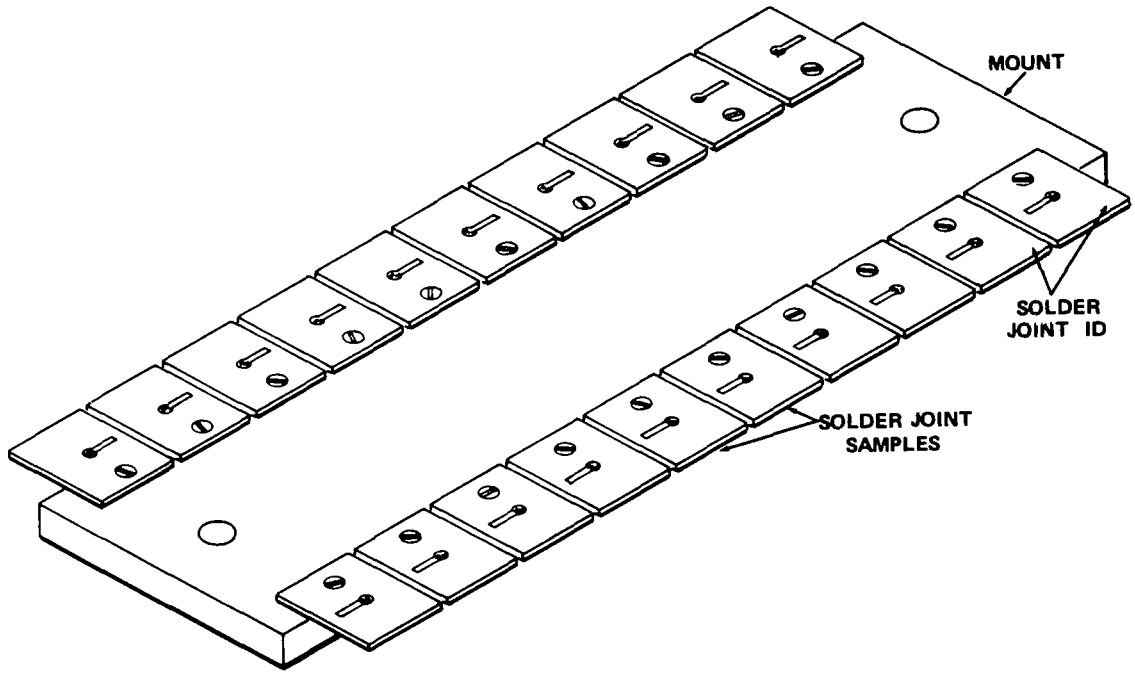

Figure 15. Mount for destructively tested solder joints.

The destructive tests described here were based on "design requirements of soldered printed wiring board assemblies" [23] as prescribed by Marshall Space Flight Center. Operating temperatures of -55°C to +100°C are specified for such assemblies. The types of solder joints employed in the thermal testing were typical of those specified in Reference 23. Rate of change of air temperature was not allowed to exceed 5°C per minute in the test chamber in which destructive testing of the solder joints was performed. A thermal cycle of 2 hours duration was chosen in which 35 minutes was required for transition from low (-55°C) to high (+100°C) temperature and an equal time was chosen for transition from high to low temperature. A 25 minute time at both high and low temperature was allowed for temperature equilibration.

A total of 12 cycles of testing could be accomplished each 24 hours for continuous operation of the environmental test chamber. The solder joints were microscopically inspected at 25, 50, 75, and 100 cycles respectively. These inspection intervals were based on previous work performed by experimenters at Marshall Space Flight Center. Inspection of the samples was made at intervals of 10 cycles after the 100th cycle because of the more rapidly changing condition of the joints. This thermal cycling schedule was continued until 190 cycles had been performed. At that juncture a large percentage of the solder joints had failed, and little additional information could be gained from further testing.

V. EXPERIMENTAL RESULTS

The results of solder joint testing demonstrated the interrelationships among the solder joint parameters, the forces applied to the joints, the change of solder joint temperature, and the survivability of solder joints. The changes in optical correlation that are caused by forces applied to the solder joints are shown in the section on mechanical testing results and in Table 6. The effect on solder joints of changes in temperature is shown in the section on thermal test results. These data and the destructive testing data, based on an arbitrarily designated numerical representation of solder joint conditions in Table 7, are presented in tabular and graphic form. The feasibility of nondestructive evaluation of solder joints is indicated in the analysis of these data.

A. Mechanical Testing Results

The proposition was made prior to mechanical testing of the solder joints that by observing the change that occurs in the optical correlation signal, information could be deduced concerning the applied force and deformation that caused the correlation change. The purpose of the mechanical testing was to obtain insight into the behavior of solder joints such that some general principles might be deduced. The numerical values of the physical parameters of these circuit boards are presented in Table 8. The tested samples were constructed such that they simulated half of a a double-sided solder joint. The mechanical force applied to a single-sided joint was equivalent to a force generated within a double-sided joint and acting equally on both sides, as in the case of the thermally tested joints.

The forces applied during the mechanical tests were as high as 6.8 N and the tests were incremented in steps of 0.227 N. All four types of solder joints (types A, B, E, and F described in Fig. 12 and Table 5) were tested in this manner. The maximum force applied to each solder joint was that required to reduce the optical correlation signal to approximately the 60 percent level. This limit permitted testing to be terminated prior to permanent deformation of the solder joint. The limit of 40 percent loss in correlation

TABLE 6. OPTICAL CORRELATION CHANGE DATA FROM THERMAL TESTING

Sample		Fractional Loss in Optical Correlation			
Board No.	Side No.	Type I	Type II	Type C	Type D
1	1	0.37	0.70	0.22	0.42
	2	0.34	0.28	0.18	0.75
2	1	0.64	0.52	0.34	0.44
	2	0.38	0.26	0.58	0.41
3	1	0.52	0.29	0.20	0.45
	2	0.24	0.10	0.37	0.28
4	1	0.34	0.25	0.45	0.46
	2	0.49	0.77	0.57	0.76
5	1	0.40	0.47	0.42	0.70
	2	0.20	0.26	0.76	0.56
6	1	0.82	0.38	0.20	0.24
	2	0.34	0.48	0.38	0.31
7	1	0.69	0.40	0.60	0.73
	2	0.37	0.08	0.23	0.56
8	1	0.48	0.46	0.14	0.50
	2	0.17	0.44	0.10	0.17
9	1	0.58	0.24	0.69	0.34
	2	0.20	0.69	0.42	0.49
10	1	0.62	0.27	0.34	0.14
	2	0.46	0.62	0.24	0.66
Average Loss		0.43	0.40	0.40	0.47

signal was taken as a safe factor to guarantee the nondestructive nature of the test. Forces that result in less than 40 percent loss in optical correlation are within the elastic limit of the solder. The results of exceeding 40 percent correlation loss were of two types. In the first type, the changes that occurred as a result of the applied force did not

TABLE 7. NUMERICAL REPRESENTATION OF SOLDER JOINT CONDITIONS

Solder Joint Conditions	Numerical Representation
Specularly reflecting surface having no graininess, or non-specularly reflecting surface having no change in graininess from the original condition based on the beginning of thermal testing.	0
Beginning of appearance of graininess or any change in the graininess of the surface from the pre-tested condition.	1
Large change in surface condition with crazed or undulatory appearance; very fine crack.	2
Appearance of large cracks or cracks extending a large portion of the distance around the solder joint lead wire.	3

Note: The numerical representation of the condition of the double-sided board is considered to be the arithmetic sum of the numerical representations of the solder joints of each of the two sides.

disappear with the removal of the force. After some hours of delay, the correlation signal would increase to some extent. However, a full recovery never occurred if the elastic limit had been exceeded. In the second type, as the force applied to the solder joint lead wire was incrementally removed, the signal displayed hysteresis with respect to the signal generated during the incremental increase in the applied force. This hysteresis was much less pronounced for joints tested to less than the 40 percent correlation signal criterion.

Twelve test solder joints of each type (types A, B, E, and F, Fig. 12 and Table 5) were tested to determine the effect of a manually induced, static force. Data from the testing of several of these samples are presented in Figures 16, 17, 18, and 19 and Tables 9, 10, 11, and 12 for the four types of solder joints tested.

The trend for all the mechanically tested solder joints was a decrease in optical correlation as the force on the lead wire was increased. In most tests the rate of decrease in correlation signal was low for small applied forces, but was considerably higher for larger applied forces.

The signal characteristics of several solder joints from the group of 48 that were mechanically tested departed radically from the majority of the data. These deviations included reversals in the slope of the optical correlation curve as a function of linearly

TABLE 8. NUMERICAL VALUES OF PHYSICAL PARAMETERS IN PRINTED CIRCUIT BOARDS

Symbol	Definition	Numerical Value	Ref.	Comment
α_w	Coefficient of expansion of wire	5×10^{-6} m/m°C	25	Kovar wire
E_w	Modulus of elasticity of wire	13.8×10^6 N/cm^2	25	Kovar wire
a_w	Radius of wire cross section	0.406 to 0.457		Manuf. Specifications. G10 epoxy with planar fiberglass reinforcement
L	Half-thickness of circuit board material	0.79 mm		
α_L	Coefficient of expansion of circuit board material	60×10^{-6} m/m°C	25	Value for axis perpendicular to plane of material
E_L	Modulus of elasticity of circuit board material	0.772×10^6 N/cm^2	25	Same as above
h_p	Solder pad thickness	0.071 mm		"2 oz copper"
a_a	Solder pad outer radius	1.27 mm		
a_b	Solder pad inner radius	0.318 mm		Nonplated holed
		0.381 mm		Plated-through holes
α_s	Coefficient of expansion of solder	24.7×10^{-6} m/m°C 30.4×10^{-6} m/m°C	26 1	Eutectic tin-lead solder
	Tensile strength – solder	5170 N/cm^2 5310 N/cm^2	26 1	Eutectic tin-lead solder
	Shear strength – solder	4270 N/cm^2 3720 N/cm^2	26 1	Eutectic tin-lead solder
	Tensile strength – copper solder joint	20 000 N/cm^2	26	
	Shear strength – copper solder joint	5510 N/cm^2	26	

Note: Creep rate for eutectic tin-lead solder at room temperature is 0.0001 inch per inch per day at 335 psi (0.0001 m/m per day at 231 N/cm^2).

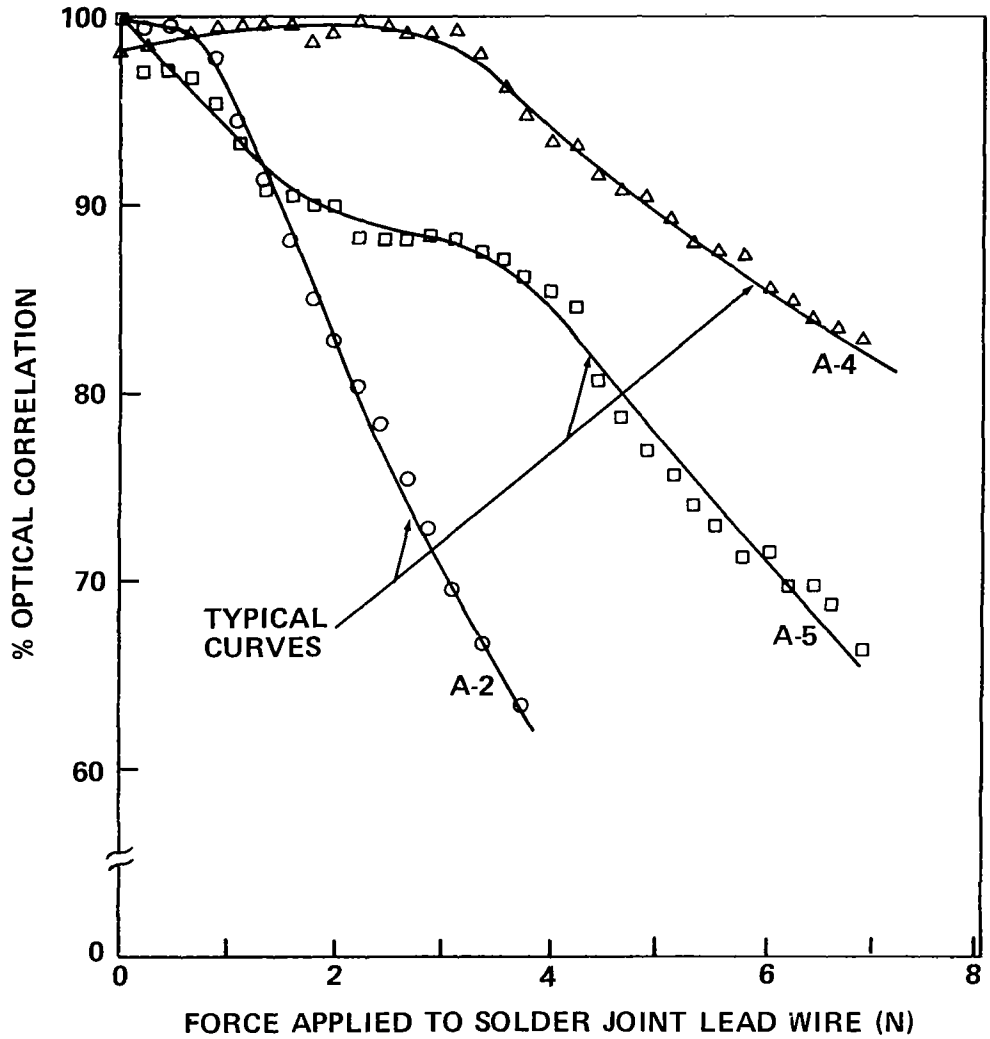

Figure 16. Optical correlation versus force for type A solder joints.

applied force. In these cases the typical downward trend in optical correlation was followed by an upward trend and finally by a second downward trend. Several solder joints that exhibited double reversals were tested again in an identical manner. The atypical behavior of the optical correlation versus applied force curves was found to have resulted from improper solder joint mounting. These irregularities of data results were not reproducible; however, the typical data curves were repeatable. Other sample joints produced only a small loss in optical correlation as force on the lead wire was increased to 6.76 N, the highest force employed in the mechanical testing. These samples, in a majority of cases, possessed physical characteristics that indicated strength of the joint in excess of the average strength of that class of joints.

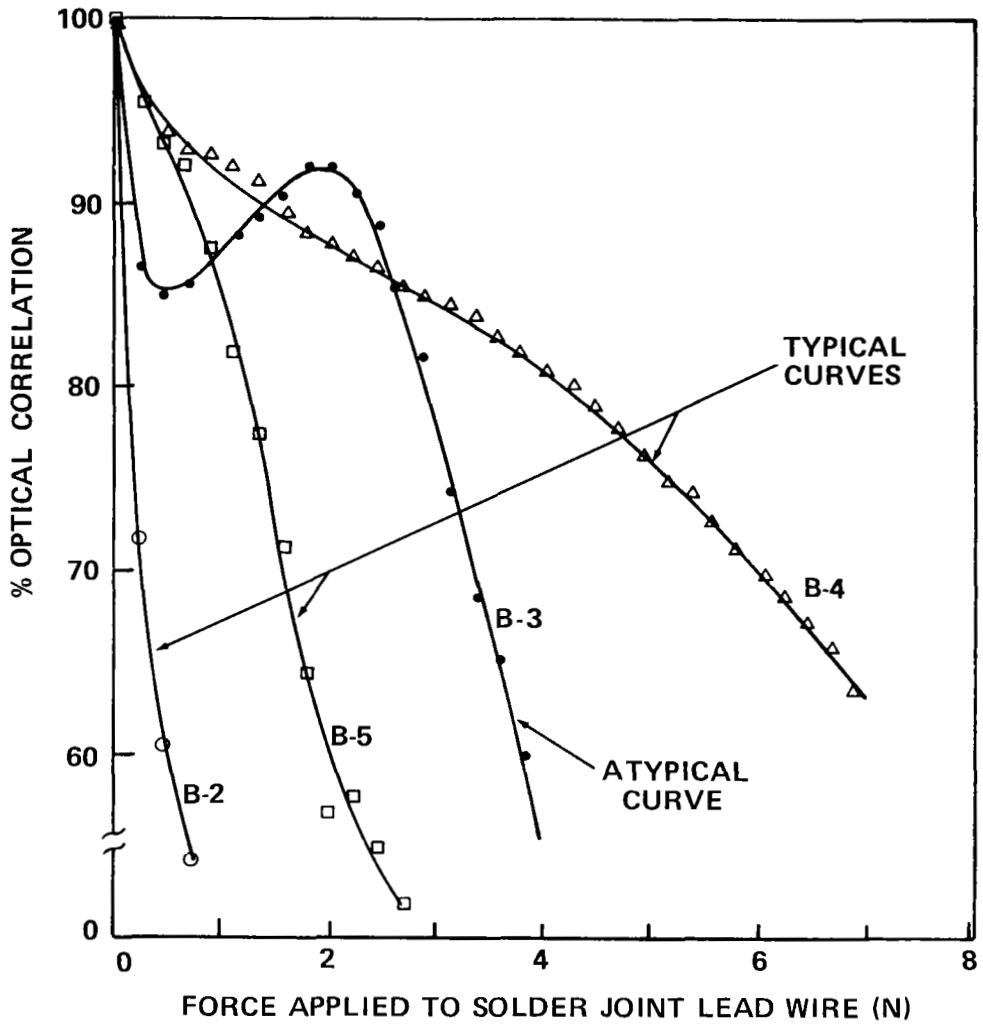

Figure 17. Optical correlation versus force for type B solder joints.

Of the four types of solder joints mechanically tested, type E and type F were the simplest in construction. A type E joint was equivalent to one-half of a double-sided joint. Double-sided joints were analyzed in Section III. This analysis was based on a double-sided stud type joint. Type F joints are more complex because they possess plated-through holes. The plating allows for a bond between the hole surface and the lead wire, thus increasing the complexity of a hypothetical model.

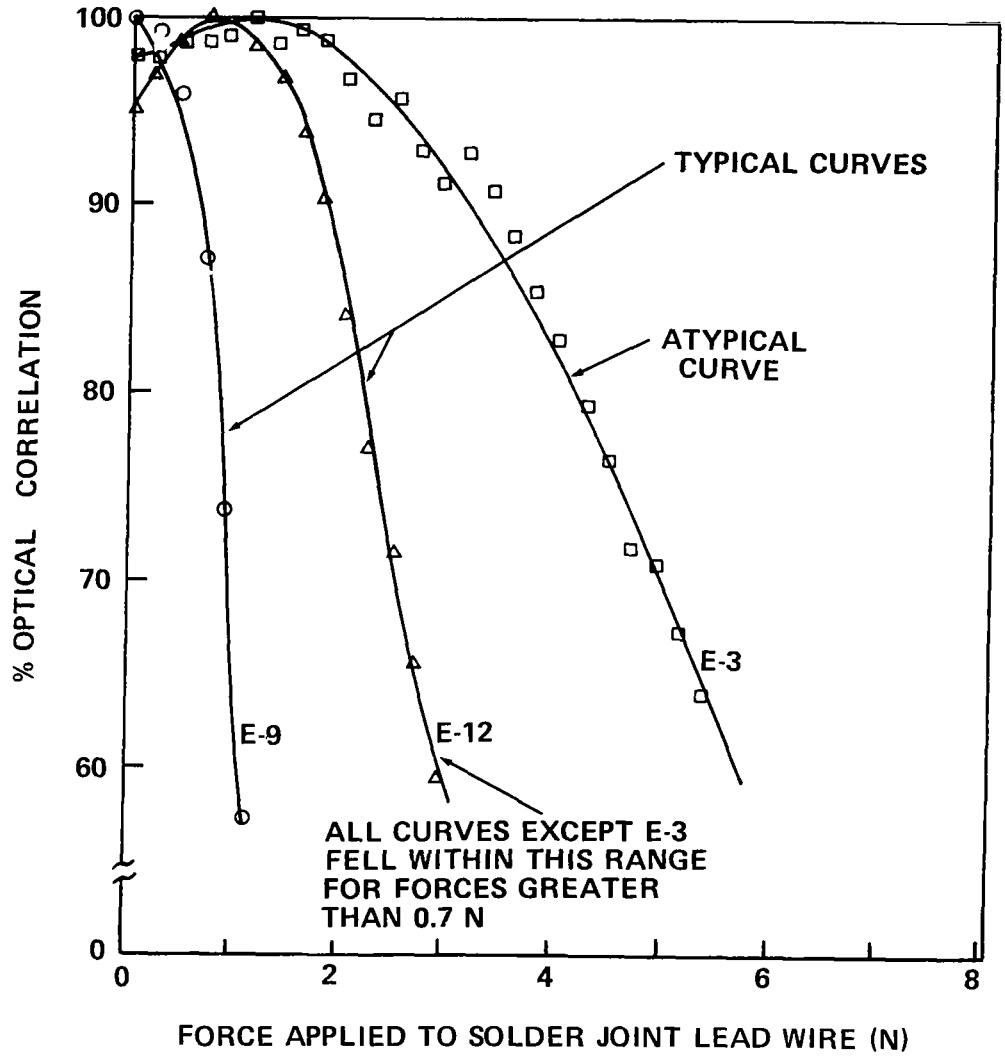

Figure 18. Optical correlation versus force for type E solder joints.

Type A and type B solder joints are more complex than types E and F. Type A and type B joints are less influenced by force applied to the lead because of mechanical support afforded by crimped lead wires. In general, the data from the 48 mechanically tested solder joints displayed optical correlation measurements that were less changed by force in crimped solder joints (types A and B) than in stud types (types E and F). Less change also occurred with plated-through (types A and F) than non-plated-through hole types (types B and E) of joints (Figs. 16 through 19).

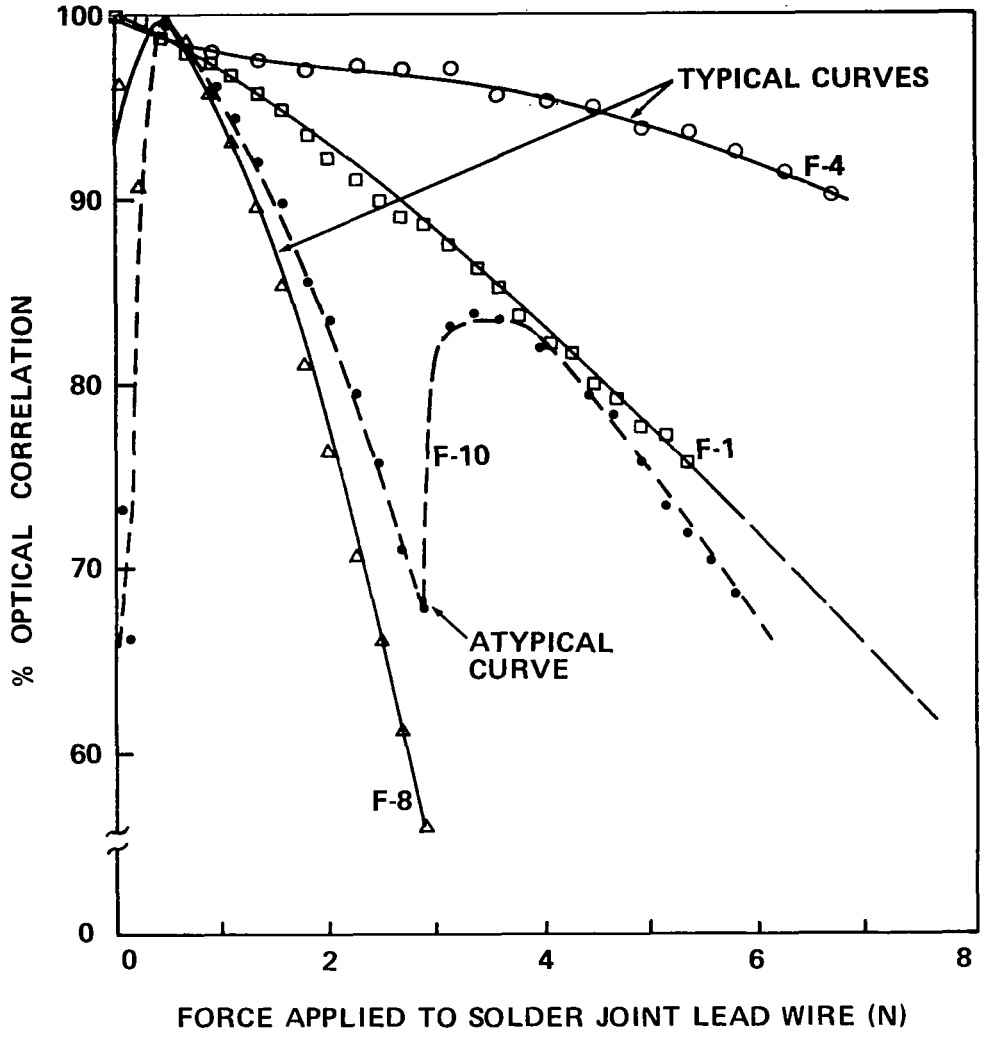

Figure 19. Optical correlation versus force for type F solder joints.

The data resulting from testing of type E solder joints display less variation from one test sample to the next than the other types of joints. The data plots from eleven of the twelve type E solder joints generally fell within the narrow range between curves E-9 and E-12 shown in Figure 18. The maximum optical correlation signal was achieved at no greater than 0.67 N for the eleven typical examples, and the curves decreased monotonically above this force level.

TABLE 9. OPTICAL CORRELATION DATA FROM THE MECHANICAL TESTING OF TYPE A SOLDER JOINTS (See Fig. 16)

Applied Force (N)	Optical Correlation (%)		
	Solder Joint A-2	Solder Joint A-4	Solder Joint A-5
0.0	100.0	98.3	100.0
0.222	99.3	98.7	97.1
0.445	99.6	99.1	97.1
0.667	99.3	99.4	96.8
0.890	97.8	99.5	95.5
1.112	94.4	99.6	93.1
1.334	91.4	99.4	91.0
1.557	88.1	99.6	90.5
1.779	84.8	98.6	90.0
2.002	82.9	99.1	90.2
2.224	80.3	100.0	88.3
2.446	78.5	99.5	88.1
2.669	75.5	99.0	88.1
2.891	72.5	99.0	88.3
3.114	69.5	99.2	88.3
3.336	66.5	97.9	87.5
3.558	63.2	96.2	87.0
3.781		94.5	86.2
4.003		93.3	85.4
4.226		93.0	84.4
4.448		91.4	80.4
4.670		90.6	78.5
4.893		90.4	76.9
5.115		89.1	75.6
5.338		87.8	74.0
5.560		87.4	72.9
5.782		87.2	71.1
6.005		85.7	71.3
6.227		84.7	69.5
6.449		83.7	69.7
6.672		83.4	68.7
6.894		82.9	66.3

TABLE 10. OPTICAL CORRELATION DATA FROM THE MECHANICAL TESTING OF TYPE B SOLDER JOINTS (See Fig. 17)

Applied Force (N)	Optical Correlation (%)			
	Solder Joint B-2	Solder Joint B-3	Solder Joint B-4	Solder Joint B-5
0.00	100.0	100.0	100.0	100.0
0.22	71.7	86.4	94.6	95.4
0.44	60.6	84.1	93.7	93.4
0.67	54.5	85.1	92.7	92.0
0.89		86.6	92.7	87.5
1.11		88.2	92.1	81.9
1.33		89.0	91.2	77.4
1.55		90.4	89.7	71.2
1.77		92.1	88.3	64.3
2.00		91.9	87.7	57.0
2.22		90.4	87.4	57.7
2.44		88.6	86.4	55.0
2.66		85.4	85.4	51.8
2.89		81.7	84.7	
3.11		74.3	84.5	
3.33		68.4	83.9	
3.55		65.0	82.6	
3.78		60.0	81.8	
4.00			80.8	
4.22			80.1	
4.44			78.9	
4.67			77.8	
4.89			76.1	
5.11			74.7	
5.33			74.3	
5.56			72.6	
5.78			71.1	
6.00			69.9	
6.22			68.6	
6.44			67.2	
6.67			65.9	
6.89			63.4	

TABLE 11. OPTICAL CORRELATION DATA FROM THE MECHANICAL TESTING OF TYPE E SOLDER JOINTS (See Fig. 18)

Applied Force (N)	Optical Correlation (%)		
	Solder Joint E-3	Solder Joint E-9	Solder Joint E-12
0.00	97.9	100.0	94.9
0.22	97.5	99.1	96.6
0.44	98.3	95.6	98.3
0.67	98.3	86.8	100.0
0.89	98.7	73.7	98.9
1.11	100.0	57.5	98.3
1.33	98.3		96.6
1.55	99.2		93.7
1.77	98.7		90.3
2.00	96.6		84.0
2.22	94.5		77.1
2.44	95.4		71.4
2.66	92.8		65.7
2.89	91.1		59.4
3.11	92.8		
3.36	90.7		
3.55	88.2		
3.78	85.2		
4.00	82.7		
4.26	79.3		
4.44	76.4		
4.67	71.7		
4.89	70.9		
5.11	67.1		
5.33	64.1		
5.56	61.6		

TABLE 12. OPTICAL CORRELATION DATA FROM THE MECHANICAL TESTING OF TYPE F SOLDER JOINTS (See Fig. 19)

Applied Force (N)	Optical Correlation (%)			
	Solder Joint F-1	Solder Joint F-4	Solder Joint F-8	Solder Joint F-10
0.00	99.9	100.0	96.2	73.3
0.22	100.0	99.2	90.8	66.0
0.44	99.0	98.9	100.0	100.0
0.67	97.8	98.7	98.5	98.0
0.89	97.3	97.9	95.8	96.5
1.11	96.8	97.1	93.1	94.2
1.33	95.9	97.6	89.7	92.0
1.55	95.0	99.2	85.5	89.8
1.77	93.6	97.1	80.9	85.6
2.00	29.3	98.1	76.3	83.4
2.22	91.2	97.3	70.6	79.2
2.44	90.0	96.8	66.0	75.4
2.66	89.2	97.1	61.1	71.0
2.89	88.6	97.1	55.7	68.2
3.11	97.4	97.1		83.5
3.33	86.4	96.3		84.0
3.55	85.0	95.7		83.5
3.78	83.7	95.5		83.0
4.00	82.2	95.2		82.3
4.22	81.8	94.9		81.3
4.44	80.0	94.9		79.9
4.67	79.2	93.6		78.4
4.89	66.6	93.8		76.6
5.11	77.0	94.1		73.4
5.33	75.7	93.8		71.8
5.56		92.3		70.3
5.70		92.5		68.5
6.00		90.7		
6.22		91.5		
6.44		90.4		
6.67		90.1		
6.89		89.1		

Type F joints (Fig. 19), differing from Type E only in the plating through of the lead wire holes, had optical correlation curves that generally fall into two families. Seven of the twelve samples yielded data similar to type E data. Four of the other five samples showed much less change in optical correlation with applied force than these seven. The remaining type F sample showed atypical behavior in that it displayed two distinct reversals in the optical correlation signal.

Data from the testing of type B solder joints (Fig. 17) did not differ greatly from the data from type E testing. However, several type B solder joint correlation measurements were less drastically affected by applied force. Two joints showed atypical double reversal in the optical correlation signal.

Data from type A solder joints showed less change in signal under mechanical testing than any other type of joint. Typical curves of these data are shown in Figure 16. One sample joint, A-7, which is not shown in Figure 16, produced an exceptionally stable signal that changed no more than 4 percent from its maximum reading.

A few test specimens containing gross imperfections were tested to obtain comparisons between the behavior of these solder joints and those meeting standard quality control specifications. These tests were designed to supplement the data from space-flight-qualified solder joints. The results, as might be expected, were erratic and were of characteristics greatly different from those of quality samples.

Construction of the stud type solder joints that were mechanically tested generally met NASA specifications. These test samples were as similar as manual construction allowed. The height of the lead wire above the printed circuit board varied over the range of 0.50 mm to 1.00 mm as a result of their manual construction. The effect of this variability in the lead height was investigated by plotting the lead height versus the rate of decrease in the optical correlation measurement with applied force. This rate of decrease was based on the change in force, ΔF, required to decrease the correlation signal from 90 percent to 70 percent (i.e., $\Delta C = 0.20$). The data curves were extrapolated over this range where required. The dashed extension of the correlation data curve F-1 in Figure 19 illustrates this extrapolation. Figure 20 shows lead height versus slope relationship for type E solder joints (Table 13).

B. Thermal Testing Results

Testing of the solder joints by the application of heat simulated conditions to which all printed circuit board electronic hardware is subjected. All electronic hardware changes temperature to some extent during storage and operation. These temperature changes induce stresses in the solder joints in a manner similar to the stresses induced by forces applied to test joints during the mechanical testing procedure of this study. The principal purpose of the thermal tests was the comparison of thermal data with actual survivability of the tested joints.

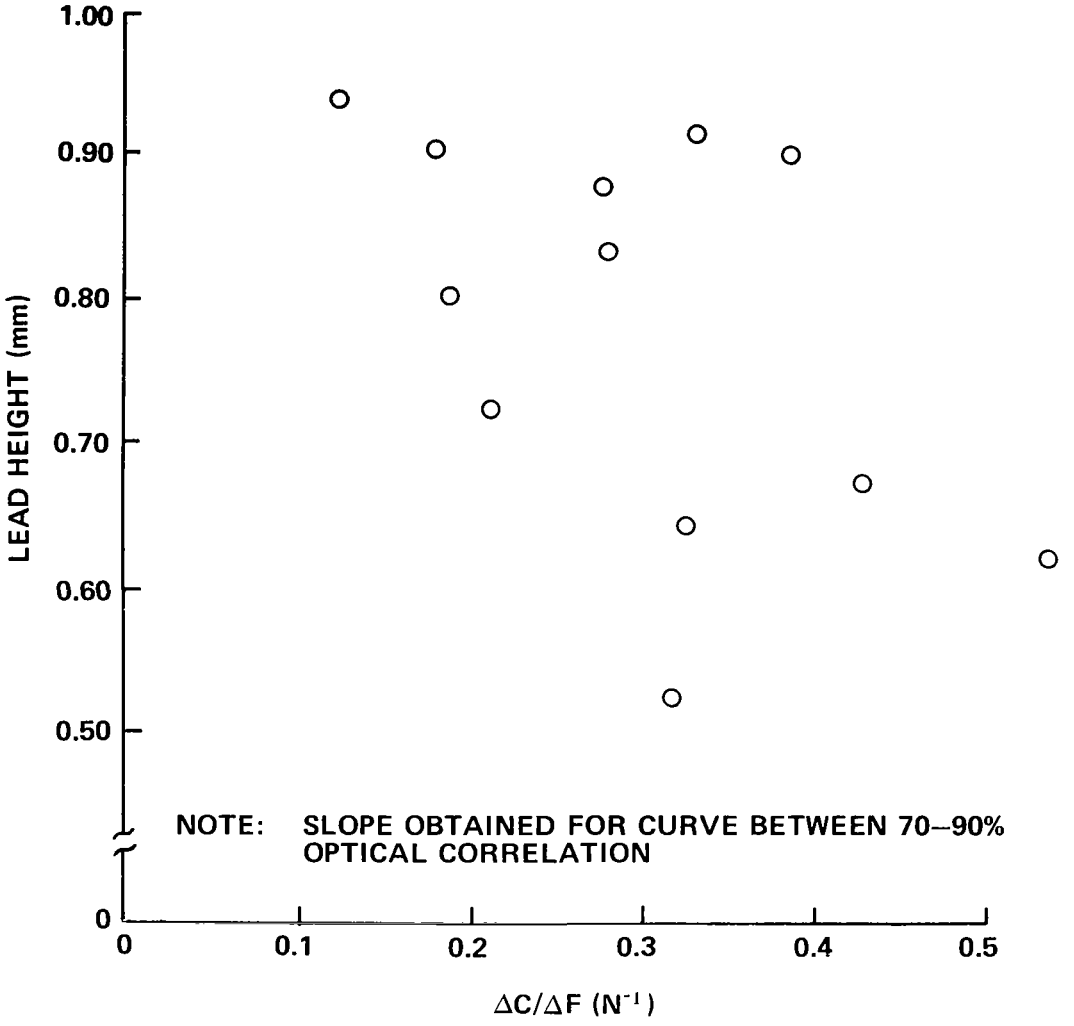

Figure 20. Lead wire height versus change in optical correlation as a function of applied force for type E solder joints – non-plated-through holes.

The types of solder joints employed in the analysis of thermal effects upon solder joints were similar to those samples tested by mechanical means. The type C and D joints (Fig. 14a and Table 5) were stud types with the former having plated-through holes, while the latter had non-plated-through holes. Similarly, types I and II (Fig. 14b and Table 5) were clinched joints, the former having non-plated-through holes. Ten samples of each of these four types of test samples were selected from 12 each that were constructed for thermal testing purposes. The 10 selected units were chosen on the basis of best adherence to manufacturing specifications and freedom from obvious defects.

TABLE 13. LEAD HEIGHT VERSUS CHANGE IN OPTICAL CORRELATION AS A FUNCTION OF APPLIED FORCE – TYPE E SOLDER JOINT DATA
(See Fig. 20)

Solder Joint	Lead Height (mm)	$\Delta C/\Delta F$ (N)
E-1	0.754	0.323
E-2	0.988	0.277
E-3	1.050	0.121
E-4	0.988	0.280
E-5	0.910	0.186
E-6	0.624	0.320
E-7	1.014	0.180
E-8	1.024	0.333
E-9	0.728	0.530
E-10	0.780	0.426
E-11	0.826	0.211
E-12	0.946	0.280

The thermal testing yielded 20 data values (changes in optical correlation, ΔC) for each type of solder joint tested, since both sides of the boards were tested. Obviously, the relationship between the two joints on opposite sides of a circuit board is strong. For example, the failure of one side such as to free the lead wire from the solder will relieve, or partially relieve, the force affecting the opposite joint. In some cases the two joints were considered as one element for purposes of analysis. In others, the data were analyzed such that each joint was considered autonomous.

Regardless of the type of solder joint being thermally tested, the temperature was raised by approximately 10°C during the heating period. From the continuous strip chart recording of the optical correlation measurement, a percentage of the initial correlation signal was obtained at 10 minutes heating time. The change in correlation, ΔC, was the single data point taken from that side of the test sample. A number of samples were duplicate tested, as discussed in the "Thermal Testing Procedure", Section IV.D, with two matched filters. An average of the two ΔC values was employed for analysis in these cases.

The resulting percentage, or fractional value, of the maximum correlation signal ranged from 97 percent to 20 percent for different thermally tested samples. The average loss in signal was approximately 40 percent for all thermally tested samples. The group average losses were: type I, 43 percent; type II, 40 percent; type C, 40 percent; and type D, 47 percent. For a sample size of 20 values of ΔC per group, the difference between type C (or type II) and type D (or type I) solder joints approached a statistically meaningful level.

Values of change in the optical correlation measurements, ΔC, that resulted from the heating of the solder joints are presented in Table 6. The ΔC value from each solder joint and the composite ΔC value from both sides of a single circuit board sample are used in the subsequent section in the comparison of the optical correlation measurements to solder joint lead height, destructive test results, and other related parameters.

C. Destructive Testing Results

Those solder joint samples that were thermally tested were subsequently destructively tested. The destructive testing procedure detailed in Section IV was typical of destructive testing procedures applied to printed circuit boards at the Marshall Space Flight Center. Types C and D solder joint samples were mounted as shown in Figure 15. Types I and II were similarly mounted. For each of the 80 individual solder joints destructively tested, a data point consisted of a microscopic inspection evaluation of each sample joint after each interval of thermal cycling.

Solder joints that undergo destructive thermal cycling incur changes in surface conditions. The microscopic inspection of the solder joints destructively tested for this study was designed to periodically monitor changes that occur as a result of destructive testing. Solder joints into which significant force levels are induced during changes in temperature exhibit a progressive change in appearance as they are thermally cycled. The orderliness of these changes allow for a multilevel classification of the condition of the solder joint (Table 7). The solder joints may, for example, be referred to as "beginning to fail," "in the process of failing," or "completely failed." This classification of degradation is qualitative and is generally followed for all samples tested.

Inspection of the printed circuit boards, which occurred periodically during thermal cycling, was accomplished by employing a binocular microscope. The solder joints were illuminated by two lamps oriented to provide as uniform a coverage as possible. A magnification factor of 10, 15, or 20 was used as necessary, some details being more easily recognized at one magnification than at another. Because of the nonplanar nature of the solder joint, the inspection included considerable turning of the solder joint in the field of view of the microscope. Shading first one light source and then the other revealed features such as cracks that might be overlooked if the subject were uniformly illuminated.

The first visual indication of the initiation of progressive deterioration of a solder joint undergoing destructive thermal cycling was the appearance of a fine grained surface texture. The first phase of the changing appearance of the solder joint was especially difficult to detect when the original surface condition was fine grained. These surface changes were the result of changes in the crystalline structure of the solder material. These changes contributed to a decrease in the total structural integrity of the solder material.

Further testing resulted in the surface graininess increasing to the point where the surface became crazed or surface undulation features appeared. Further thermal cycling produced very fine cracks which were usually oriented along the undulatory features. These cracks were difficult to locate and to assess in terms of penetration depth. Therefore, an uncertainty in the classification of solder joint deterioration could possibly result. These fine cracks tended to grow in both length and depth as thermal cycling continued. The cracks tended to propagate in a circular pattern for solder joints of the stud type. After sufficient cycling the cracks normally encircled the lead wire. The location of this encircling crack was generally nearer the lead wire than it was to the outer circumference of the solder pad. For clinched type solder joints, cracks normally occur opposite the clinched wire at the base of the lead wire, at the point indicated in Figure 4, and along the wire away from the lead wire hole.

A qualitative evaluation of the condition of each of the thermally tested solder joints was made as destructive testing of the solder joints progressed and as inspections were accomplished. These evaluations were subsequently assigned numerical values based upon the condition of the solder joints. The numerical values assigned to the various conditions had no quantitative significance other than to represent the stage to which that solder joint had deteriorated. Table 7 lists the conditions that normally occur in a solder joint, as it undergoes thermal cycling, in the order in which they occur. Numerical values from zero to three represented the stages of solder joint deterioration. The condition of joints of a double-sided circuit board was represented by the sum of the numerical representations of the condition of each of the sides.

Inspection of the solder joints after 25, 50, and 75 cycles revealed minimal change in the surface condition that might indicate impending structural failure. After 100 cycles, some surface texture changes were beginning to occur; one each of the type C and D solder joints had begun to crack. Additional data taken after 110 and 120 thermal cycles showed increased deterioration of the solder joints.

Data from type C and type D solder joints are presented in Figures 21 and 22 and in Tables 14 and 15. The data from type C solder joints resulted from the inspection of the joints at 120, 140, and 170 thermal cycles. For type D solder joints the data were taken after 120, 150, and 180 thermal cycles. These intervals in the thermal test sequence gave representative data indicative of the transition in surface condition between the first significant surface changes after 100 cycles and the limit of change that was approached at approximately 190 cycles.

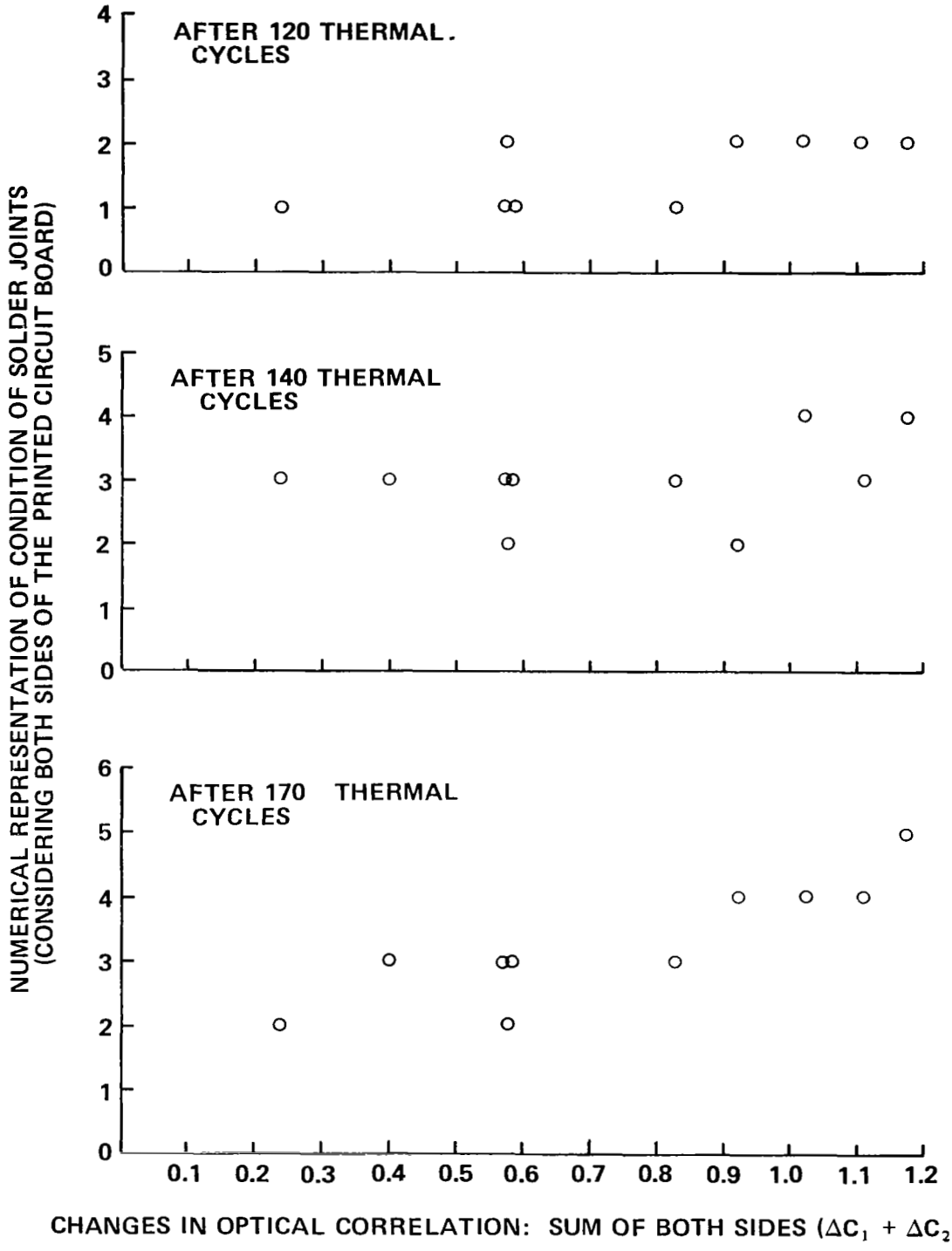

Figure 21. Results of thermal testing of type C solder joints.

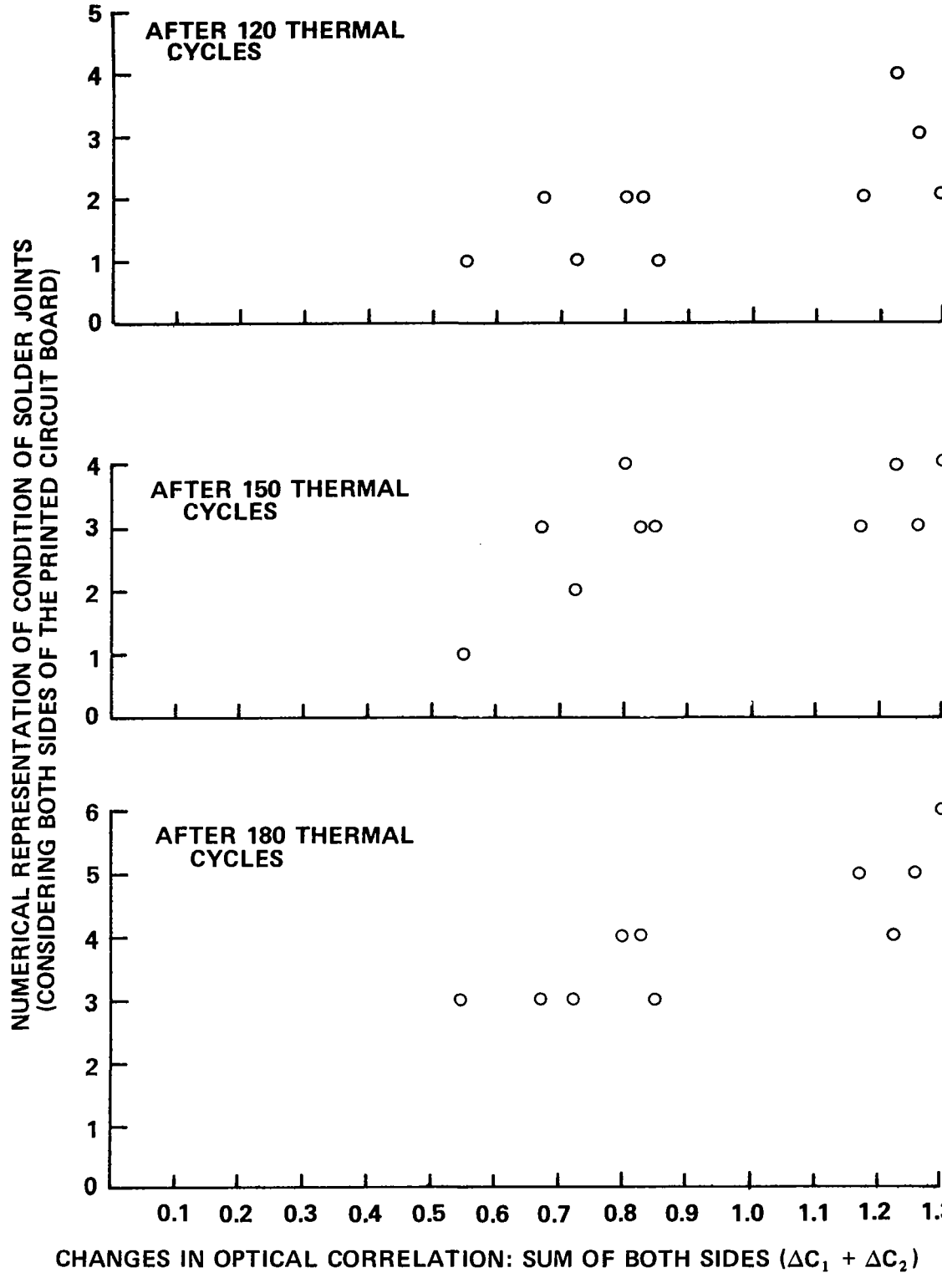

Figure 22. Results of thermal testing of type D solder joints.

TABLE 14. DATA ON RESULTS OF DESTRUCTIVE TESTING OF TYPE C SOLDER JOINTS (See Fig. 21)

Solder Joint Number	Loss of Optical Correlation ($\Delta C_1 + \Delta C_2$)	Numerical Representation of Condition		
		After 120 Cycles	After 140 Cycles	After 170 Cycles
C-1	0.40	0	3	3
C-2	0.92	2	2	4
C-3	0.57	1	3	3
C-4	1.02	2	4	4
C-5	1.18	2	4	5
C-6	0.58	1	2	2
C-7	0.83	1	3	3
C-8	0.24	1	3	2
C-9	1.11	2	3	4
C-10	0.58	2	3	3

TABLE 15. DATA ON RESULTS OF DESTRUCTIVE TESTING OF TYPE D SOLDER JOINTS (See Fig. 22)

Solder Joint Number	Loss of Optical Correlation ($\Delta C_1 + \Delta C_2$)	Numerical Representation of Condition		
		After 120 Cycles	After 150 Cycles	After 180 Cycles
D-1	1.17	2	3	3
D-2	0.85	1	3	3
D-3	0.73	1	2	3
D-4	1.22	4	4	4
D-5	1.26	3	3	5
D-6	0.55	1	1	3
D-7	1.29	2	4	6
D-8	0.67	2	3	3
D-9	0.83	2	3	4
D-10	0.80	2	4	4

Figures 21 and 22 are presentations of data in which the changes in optical correlation measurements were composites ($\Delta C_1 + \Delta C_2$) of the changes for both solder joints of each sample of type C and D printed circuit boards; likewise, the conditions of the joints were composites. A plot of the condition of each side versus the optical correlation measurement change for that side was also made but not included in the figures. Analysis of the results of single-side correlation were comparable to the composite data shown in Figures 21 and 22.

Type I and type II solder joints displayed a progressive increase in the thermal cycling effect on the condition of the solder joints in a manner similar to the type C and D solder joints. The scatter of the data was greater as is discussed in Section VI.

VI. DISCUSSION OF RESULTS

The experimental data presented in the preceding section resulted from mechanical and thermal nondestructive testing and from destructive thermal testing of solder joints. The testing procedures were designed to determine the behavior of solder joints subjected to force. The feasibility of nondestructive evaluation of solder joints via optical correlation measurements was assessed from this behavior.

The mechanical tests were directed towards determining the effect of incremented changes in force applied to the solder joint lead wires. Force, from whatever source, degrades the structural integrity of solder joints. The ability of optical correlation to detect significant forces was ascertained through mechanical tests. A determination of the limit to which solder joints could be stressed without permanent damage also was made through these tests. Mechanical application of force was chosen as a test method because of the ease with which the force could be controlled and measured.

Thermal testing simulated the effect of normal operation on a printed circuit board. Because of temperature change, forces were induced internal to the solder joints. By varying solder joint test sample temperatures a few degrees centigrade, nondestructive, reversible changes occurred. Optical correlation measurements of these changes provided an assessment of the effect of the temperature change. The destructive thermal tests were performed on those samples that had been nondestructively thermally tested. The purpose of these destructive tests was to establish the relationship between the survivability of solder joints as predicted by nondestructive thermal tests and the actual durability of the solder joints during extreme temperature fluctuations.

Testing of the solder joint samples by the application of mechanically applied force yielded two significant results. Firstly, as force was applied to the solder joints, the optical correlation intensity decreased in proportion to the force applied. Secondly, the proportionality between force change and optical correlation change varied from one

solder joint sample to the next, although they were of identical manufacturing specifications. The first result is conducive to the feasibility of nondestructive evaluation since greater force levels induced by temperature changes in an electronic package would produce a proportionally larger change in an optical correlation measurement. The variability of the proportionality between force change and optical correlation change from one solder joint to the next has been shown to depend in part on the manner in which the joint was constructed. Solder joints weakened by short lead wire lengths above the solder pad showed larger changes in optical correlation when tensioned than did stronger solder joints having longer lead wires.

A majority of the solder joints that were mechanically tested displayed similar behavior. This behavior was a decreasing optical correlation intensity with increasing applied force. The degree of linearity of the plot of these data was approximately the same although the slope of the optical correlation versus force curve varied by as much as a factor of ten. Although the four types of solder joints that were mechanically tested were significantly different in characteristics, the optical correlation measurements were similar in nature. A straight line approximation of the data obtained from these typical solder joints represented the data to a high degree. The exceptions to this typical behavior of the solder joints were those in which a maximum occurred in the optical correlation versus applied force curve and those with erratic reversals in that curve. However, those curves with maxima are shown to result from effects introduced by the measurement.

Figures 16 through 19 illustrate optical correlation versus applied force curves having typically linear shape as well as having maxima characteristics. These maxima are related to the response to force for some solder joints in which the optical correlation measurement increased as force was applied. This result apparently indicated a correlation value higher than the autocorrelation value, an occurrence not expected. The conclusion drawn was that the condition of the solder joint with no force applied was not a condition for autocorrelation. The temperature difference between the solder joint recorded holographically and as illuminated for correlation measurements was as great as 2°C. Prior to exposure, the solder joint had time to attain room temperature. The duration of illumination of the solder joint during construction of the matched filter was of the order of a fraction of a second in normal circumstances. Under these circumstances the duration of exposure of the solder joint to heating by the laser light was insufficient to significantly raise the temperature of the solder joint during exposure. Therefore the matched filter was optimum for a solder joint at room temperature. During optical correlation measurements, however, the solder joint was continuously heated by the laser light. The optical correlation did not constitute autocorrelation when no force was applied because of the heat induced physical changes in the solder joint.

The effect of the laser light heating of the solder joint sample was measured in the following manner. A matched filter was constructed and reinstalled in the optical system. The temperature of the solder joint and the optical correlation measurement were simultaneously observed as the solder joint was reilluminated. The rise in temperature of the solder joint was followed closely in time by a decrease in the correlation signal. This

effect reduced the optical correlation measurement at zero applied force – a natural consequence of the heat induced surface displacement of the solder joint. The ramification of a zero force condition not producing autocorrelation was that some positive force condition may exhibit a higher correlation value than the zero force condition. Heating expanded the test sample in a direction opposite to the direction in which compression occurred as force was applied. This displacement was effectively reduced by force applied to the lead wire. This effective reduction in surface displacement caused an increase in optical correlation with applied force as shown in curve E-12 on Figure 18.

Indicative of this phenomenon was the relationship between the height of the solder joint lead wires above the solder pad and the amplitudes of the maxima in the correlation curves relative to zero force correlation. A qualitative appraisal of this characteristic allowed the twelve samples of the type E solder joints to be divided into two groups of six each. One group contained the solder joints having the most pronounced maxima in the force versus optical correlation curves and the other had the least pronounced maxima. Five of the six solder joints with the greatest maxima also were among the 50 percent of the solder joints with the longest lead wire heights above the solder pads. Thus it would appear that the longer lead wires (normally accompanied by greater heights of solder) expanded more as the temperature increased and required more force to compress the solder joint back to its original position than the shorter lead wires.

Results of solder joint testing, regardless of the means by which force is applied to the joint, must take into consideration the nature of solder and its tendency to creep. Creep [22] as observed in solder is illustrated in Figure 23. This figure represents the strain versus time response of solder to a constant stress. The creep characteristic of a material is normally stated in pounds per square inch required to produce a creep rate of 0.0001 inches per inch per day [22]. Creep is a time dependent function and its magnitude is additive to the elastic stress-strain relationships of materials. Because of creep, a material may fail as the result of the application of stress which is only a fraction of the ultimate tensile or shear strength of the material; failure may require a large amount of time, however.

A small load applied to solder initially produces a rapidly increasing amount of strain. At room temperature the strain rate slows to a relatively fixed value in the time range "A" to "B" as shown in Figure 23. At time "B" the strain rate will again increase until failure of the material occurs, if the applied stress and/or the temperature is sufficiently high. The initial behavior of strain between time zero and time "A" is dominated by the plastic deformation resulting from structural rearrangements in the material. Depending on the stress level in the material, lattice rearrangements up to a certain energy level (based on the applied stress) will occur. On completion of this process, referred to as work hardening, no increase in strain should occur. However, a continuing, temperature dependent process allows for further strain. This process does not affect the stress-strain relationship in any significant degree for temperatures below

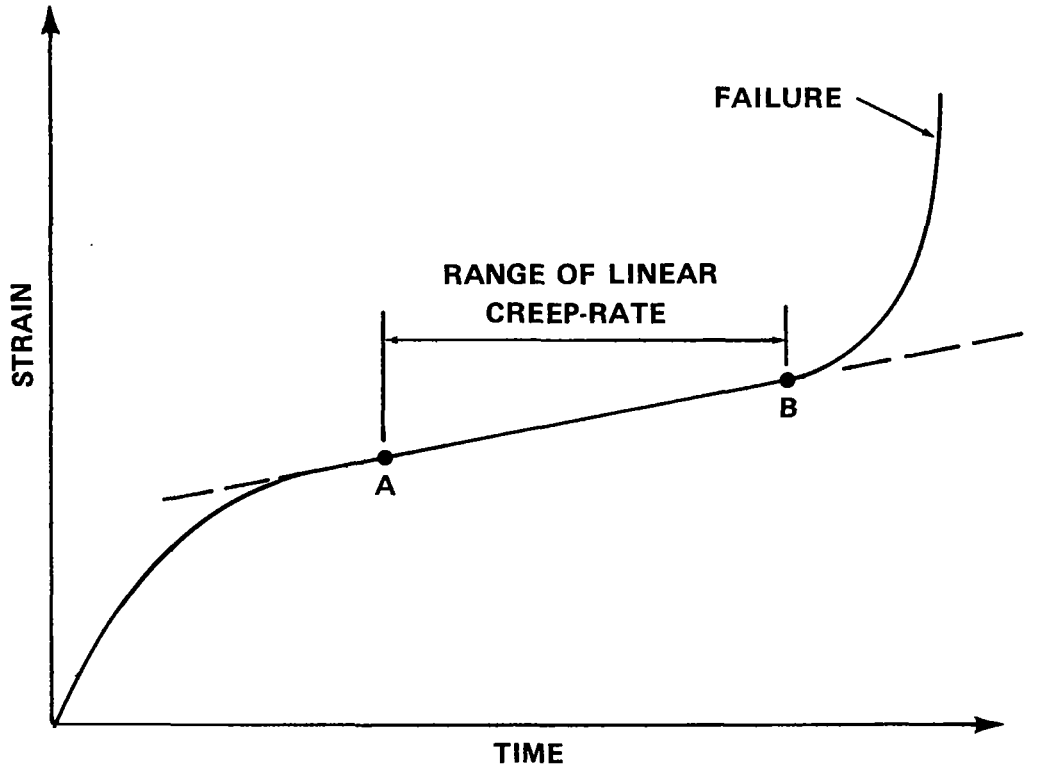

Figure 23. Creep rate characteristic of solder under constant stress.

one-third the melting temperature of the material. Room temperature, however, is approximately two-thirds of the melting temperature of eutectic lead-tin solder. The thermally activated process of dislocation motion provides a mechanism by which strain increases in the region from "A" to "B" in Figure 23.

Testing of the solder joints by the application of a static load demonstrated a rapid initial response followed by a slow continuing response to applied force. The level of the forces used in these tests was such that the slow, long term response could be neglected if approximately one-half minute was allowed between changing of force and recording of the correlation measurement. The slow, long term response required that a solder joint should be completely force tested in less than 20 minutes to minimize the effects of creep.

For the particular configuration of the solder joints used in this study, another factor contributed to the complex behavior of the joints. The Kovar wire, composed of nickel and copper, was gold plated to minimize oxidation of the wire during the period between manufacture and use. These wires were obtained from transistors. Typical

preparation of these wires for space use includes dipping or tinning the leads to remove the gold plating prior to soldering. The preparation of the lead wires for this study did not include removal of the gold plating.

In soldering of gold surfaces, the dihedral angle of wetting (a measure of the wettability of the surface) has been found to be high [24]. In comparison the dihedral angle between a tinned, or solder coated, copper surface and solder approaches zero. In the latter case, good bonding results with minimal "skips" (areas in which no solder bonds to the surface). Gold from the lead wire dissolved in the liquid solder causes an increase in the brittleness of the solder into which it diffuses [25]. Tests showed that a ternary alloy of approximately eutectic tin-lead solder to which 10 to 15 percent gold has been added is extremely brittle. Shear tests showed that this ternary alloy increased slightly in shear strength with 2.5 percent gold but decreased with greater percentages. In summary, the use of gold plated lead wire deviated from space electronic hardware assembly specifications. However, the solder joints tested were typical of those in most high quality commercial printed circuit board assemblies.

The mechanical application of force to the lead wire of type E solder joints (Table 5) will induce a shear stress, τ, as shown in Figure 6. A stress, σ_W, on the cross sectional area of the wire and a stress, σ_L, on the solder pad are also introduced. The maximum shear stress, τ_{max}, is expressed as $\tau_{max} = F/a_b h_w$. For joints of the configuration tested, τ_{max} will be between 0.97×10^3 and 1.94×10^3 N cm^{-2} N^{-1} applied force corresponding to solder joints with lead wire heights between 1.0 and 0.5 mm. Those solder joints with the longer leads provided greater load bearing area and thus reduced the maximum shear stress. This fact is supported by the information in Figures 24 and 25 and Tables 16 and 17. Figure 24 indicates the tendency for solder joints possessing short leads to show larger changes in optical correlation with heating than joints possessing longer leads. This trend is also present for data shown in Figure 25, although less strongly than for data shown in Figure 24. The effect of longer lead wires and a proportionately lower shear stress was also a proportionately smaller change in optical correlation as a result of heat induced forces in the joints.

For plated-through hole, stud type solder joints (type F), the stress created by mechanical force on the lead wire was considerably different from that for the type E solder joints. Solder may "wick" through a plated-through hole by capillary action. This wicking effect is particularly strong for tinned wires, or equivalently, for wires that have been unsoldered and then resoldered. Data from mechanical testing of one of the solder joints (curve F-4, Fig. 19) indicated a loss of optical correlation of only 10 percent at 6.67 N applied force on the lead wire. No other type F joint exhibited less correlation loss. It was found that of all these solder joints, the F-4 sample had the greatest amount of solder wicked through and accumulated around the lead wire. The load bearing area, therefore, varied greatly among solder joints with plated-through holes. Feed-through holes, which were well filled with solder, more widely distributed the load with a

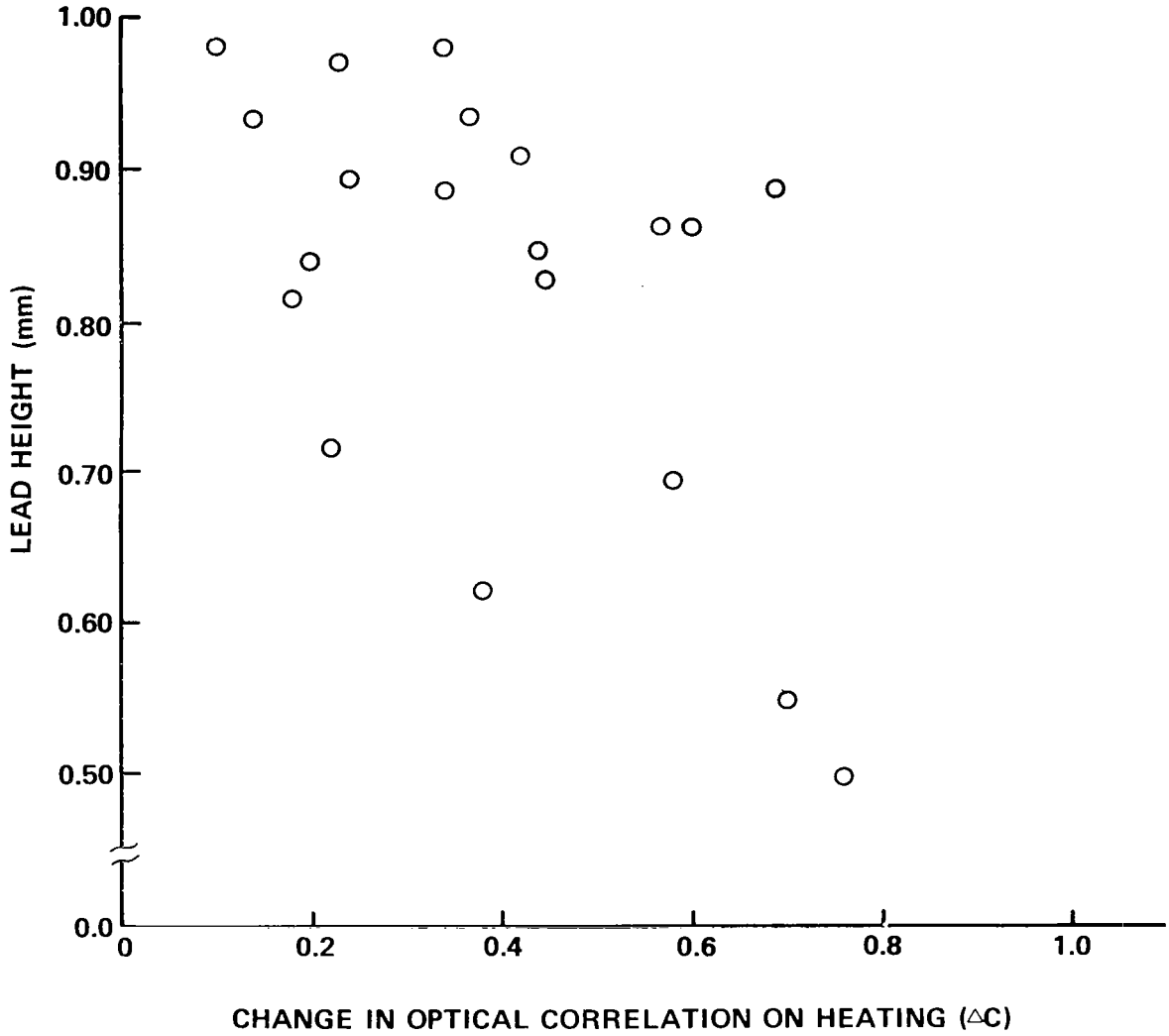

Figure 24. Lead wire height versus change in optical correlation for heated type C solder joints -- plated-through holes.

resulting reduction in the maximum stress level present in the joint. The optical correlation measurements on stud type joints with or without plated-through holes reflected the degree to which shear stress was present in the joints.

The variability of shear stress per unit applied force as a function of lead wire height and variability of solder wicking were only two factors that contributed to the differences in the behavior of solder joints when force was applied. The strength of

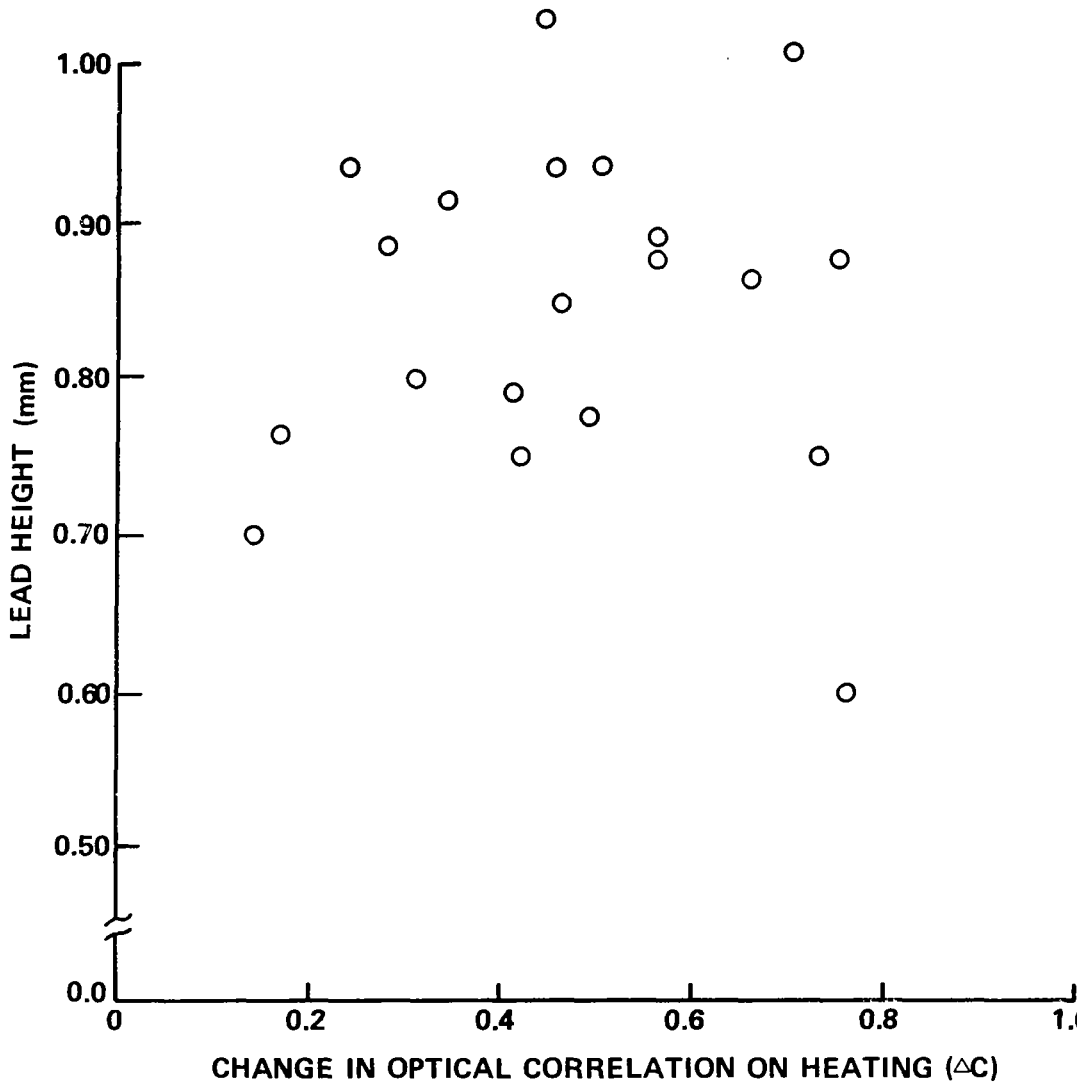

Figure 25. Lead wire height versus change in optical correlation for heated type D solder joints – non-plated-through holes.

solder-copper junctions is greater than the strength of bulk solder [26]. Implicit in this information is the effect of copper impurity in the solder. Reference 22 indicates test results showing increased creep resistance with addition of copper impurities to eutectic tin-lead solder. The degree to which copper impurities are dissolved into the liquid solder during the soldering process and the depth of the diffusion depend primarily upon the temperature to which the junction is heated and the length of time that temperature is maintained. Because of these dependencies and because of the physical process by which solder joints are hand soldered, the properties of solders in different joints varied

TABLE 16. DATA ON LEAD HEIGHT VERSUS CHANGE IN OPTICAL CORRELATION FOR HEATED TYPE C SOLDER JOINTS
(See Fig. 24)

Solder Joint Number	Circuit Board Side Number	Change in Optical Correlation on Heating, ΔC	Solder Joint Lead Height (mm)
C-1	1	0.22	0.787
	2	0.18	0.889
C-2	1	0.34	0.965
	2	0.58	0.762
C-3	1	0.20	0.609
	2	0.37	1.016
C-4	1	0.45	0.904
	2	0.57	0.940
C-5	1	0.42	0.991
	2	0.76	0.559
C-6	1	0.20	0.914
	2	0.38	0.686
C-7	1	0.60	0.940
	2	0.23	1.057
C-8	1	0.14	1.016
	2	0.10	1.067
C-9	1	0.69	0.965
	2	0.42	0.925
C-10	1	0.34	1.067
	2	0.24	0.975

TABLE 17. DATA ON LEAD HEIGHT VERSUS CHANGE IN OPTICAL CORRELATION FOR HEATED TYPE C SOLDER JOINTS
(See Fig. 25)

Solder Joint Number	Circuit Board Side Number	Change in Optical Correlation on Heating, ΔC	Solder Joint Lead Height (mm)
D-1	1	0.42	0.874
	2	0.75	0.955
D-2	1	0.44	0.118
	2	0.41	0.864
D-3	1	0.45	1.016
	2	0.28	0.965
D-4	1	0.46	0.874
	2	0.76	0.660
D-5	1	0.70	1.092
	2	0.56	0.965
D-6	1	0.24	1.016
	2	0.31	0.874
D-7	1	0.73	0.823
	2	0.56	0.955
D-8	1	0.50	1.016
	2	0.17	0.838
D-9	1	0.34	0.991
	2	0.49	0.848
D-10	1	0.14	0.772
	2	0.66	0.940

significantly. All these factors affected the strength and survivability of solder joints. Indication of this variability is seen in the optical correlation measurements of the mechanically tested solder joints (Figs. 16 through 19).

The mechanism by which crimped type solder joints constrained the movement that would be induced into the lead wire by the applied force was substantially different from that of the stud type joints. The distribution of forces within the solder was also different. The crimping of a lead wire provided the joint with contact between printed circuit board and wire in which solder was not the principal transmitting medium. This lead wire-to-copper contact had the effect of providing a solder joint strength based on the strength of the lead wire and circuit board material instead of the strength of the solder alone. However, the solder joint was weakened by the reduction in lead wire height over which the solder could support the wire.

The degree to which the crimped wire was in contact with the solder pad varied considerably as a result of manufacturing variability. These factors caused each of the crimped type solder joints to perform differently when subject to loads. This performance variability is seen in the data resulting from mechanical force testing of crimped solder joints (type A and type B, Figs. 16 and 17, Tables 9 and 10). Both the shape and the scale of the response to force of the optical correlation measurements differed in these samples more than in the stud type samples (type E and type F, Figs. 18 and 19, Tables 11 and 12). The increased number of factors that affect the performance of clinched type solder joints caused this difference in performance.

Stud and crimped solder joints having plated and nonplated holes were constructed for the purpose of thermal testing. For each type of solder joint an increase in temperature expanded the circuit board material 12 times as much as the lead wire was expanded (Table 8). This resulted in the lead wire being stretched and the circuit board material being compressed such that the two components maintained approximately equal lengths. The forces that caused stretching and compression were coupled through shear stress by the solder between the lead wire and the circuit board. These forces were defined in equation (73), which is restated below:

$$F = \frac{(\alpha_L - \alpha_w)\,\Delta T}{\frac{l}{E_w A_w} + \frac{l}{E_L A_p}} \quad ,$$

where the symbols are defined in Table 8. The values of the parameters for the components employed in the circuit board assembly were temperature dependent. Those values of the parameters for the components at 25°C were employed here because that was the ambient temperature during thermal testing. The force, F, generated by a change in temperature, ΔT, was:

$$F = (0.712\ N/°C)\ \Delta T \qquad (81)$$

The temperature of the solder joint was raised by approximately 10°C during the thermal tests. The force induced by the temperature change was approximately 7.1 N. The force to which the thermally tested joints were loaded was approximately the maximum to which any of the mechanically tested joints were tested. The force applied to the mechanically tested joints remained unchanged even if creep occurred in the solder. However, creep in the thermally tested solder joints reduced the force level in the joints. Without the creep characteristic of solder the tensile and shear strengths of the solder in the thermally tested solder joints would be exceeded with small changes in temperature.

The results of the thermal testing as shown in Table 6 differed from the results of mechanical testing in several respects. The loss in correlation might be expected to be higher for all thermally tested samples if theoretical force levels predicted for a 10°C change in temperature were realized. The effect of creep had to be considered, however. The reduction of force levels resulting from creep was not easily analyzed or calculated. As will be seen in the discussion of destructive testing results, calculated forces many times the strength of the solder material did not immediately produce fracture. Plastic deformation provided accommodation for large internal forces.

The data from thermal testing (Table 6) contained considerably less scatter than data from mechanical testing with approximately equivalent forces. These data are explained in terms of the creep effect. For those solder joints that incurred comparatively low maximum shear stress (based on longer lead wires above the solder pad) the effect of creep did not reduce this stress by a large percentage. A relatively larger amount of the shear stress was relieved for solder joints in which shear stress resulted from the particular construction characteristics of the joint. The loss in optical correlation was larger but not proportionally larger.

The wicking of the solder through the holes contributed to the high variability in the results of mechanically tested solder joints. Those solder joints that were so tested had solder on only one solder pad, on the pad and through the hole, or on both pads and through the hole. This configurational variation was not true for the thermally tested solder joints; the solder in these joints was on both sides of the circuit board. Also, soldering both sides of the board more reliably produced the capillary action through the holes than did soldering on one side alone.

Little information is available concerning the nature of creep in solder; that which is available involves room temperature conditions. The single value defining creep for solder is normally given as that stress level required for a 0.0001 inch per inch per day creep rate. This definition does not consider the relationship of creep rate change to changes in stress nor to temperature dependency of creep. Thus, more detailed information is required for the understanding of the effects of large temperature excursions on the solder joints, for example, a -55°C to +100°C temperature cycling test.

Thermal cycling between -55°C and 25°C was considerably more destructive to the solder joint than thermal cycling between 25°C and 100°C according to Marshall Space Flight Center tests. This fact indicates the effect of a lower value of circuit board coefficient of elasticity, E_L, at higher temperatures and a higher creep rate for solder at the higher temperatures.

The destructive thermal test data obtained from a series of large excursion (-55°C to 100°C) temperature cycles did not differentiate between the effects of high and low temperature creep dependence. The net effect of a series of cycles was observed and recorded. The theoretical internal force induced into the solder joint by a temperature decrease from 25°C to -55°C, was approximately 53 N. The destructive test data in Figures 21 and 22, and Tables 14 and 15, show a high survival rate for the solder joints tested between the temperature levels of -55°C and +100°C. This survival rate demonstrates that the calculated stress level (exceeding ten times the ultimate yield strength of the solder) did not occur. Creep in the solder accommodated the forces generated, which substantially extended the solder lifetime beyond the calculated limits. The mechanism of failure, then, must have been fatigue resulting from a number of thermal cycles and not the result of forces that exceeded the strength of the material.

The relationship between the optical correlation measurements made on the thermally tested solder joints and the manner in which they failed during the destructive testing was of prime importance. The thermally tested stud type solder joints showed a definite relation between the time at which they failed, or showed signs of failing, and the amount of loss in the optical correlation measurement when the temperature was increased by 10°C (Figs. 21 and 22, Tables 14 and 15). For thermally tested, clinched type solder joints this definite relation did not exist. No readily identifiable indication of the survivability of the crimped solder joints was provided by the thermal tests. However, mechanical tests yielded data indicating increased loss in optical correlation with increased force for clinched solder joints. As an indication of force present in a clinched solder joint, optical correlation may be indicative of the survivability of clinched solder joints also.

Data from the nondestructive thermal testing of stud type solder joints supplied inadequate information to determine with absolute certainty the order in which the solder joints would fail. The relative susceptibility of these solder joints to failure could be deduced from the data. Figures 24 and 25, showing the relationship between solder joint lead wire height and change in correlation with heating, indicate the relative susceptibility to failure. The survivability of solder joints has a demonstrable relationship to lead wire heights [5]. For this reason close tolerances on lead wire height is provided for in various circuit board assembly specifications.

VII. CONCLUSIONS

The optical correlation system that was developed for this study possessed significant improvements over previously available systems. The electro-optic and electronic components provided correlation measurements with improved signal-to-noise ratio, stability, and repeatability. A new approach to the construction of Vander Lugt holographic filters was perfected leading to high efficiency, temporally stable filters. The determination of both short term and long term behavior of solder joints was made possible by these filter improvements.

Optical correlation measurements were made of reversible changes in the condition of the subject solder joint. These measurements showed approximately linear response to force induced into the solder joints. The quality and type of construction of the solder joints was found to affect the correlation measurements. Those solder joints of above average strength responded less than joints of below average strength. Optical correlation measurements, therefore, indicated both the presence of force induced into the solder joint and the degree to which the joint was adversely affected by that force.

Data from the destructive testing of several solder joints were compared with data from nondestructive testing of the same joints. Thermal excitation was utilized in both the destructive and nondestructive tests. These tests simulated extreme and minimal thermal excursions, respectively. The data comparison showed conclusively that for the solder joints tested the propensity for a solder joint to fail under thermal cycling was indicated in the results of the nondestructive testing of that joint.

In this study optical correlation measurements were made separately on solder joints of varying structural strengths and on solder joints subject to various levels of force. Both of these effects normally appear simultaneously in solder joints on standard electronic printed circuit boards. Therefore, it is proposed that an extension of this work would include evaluation of a typical circuit board to determine the effects of both influences acting simultaneously.

George C. Marshall Space Flight Center
National Aeronautics and Space Administration
Marshall Space Flight Center, Alabama 35812 August 15, 1975
909-54-50

REFERENCES

1. Investigation of Solder Joints. Lockheed Missiles and Space Company, November, 1960.

2. An Evaluation of the Plated-Thru Hole. Burroughs Corporation, Military Electronic Computer Division, 1965.

3. Illustrations of Solder Joints and Tinned Circuit Boards. Boeing Company, February, 1963.

4. Investigation of Solder Cracking Problems on Printed Circuit Boards. NASA TMX-53653, September, 1967.

5. Development of Highly Reliable Solder Joints for Printed Circuit Boards. Final Report, Westinghouse Defense and Space Center, Aerospace Division, 1968.

6, Verification of Existing Design Requirements for Soldering Printed Circuit Board Assemblies. Final Report, General Electric, Re-entry and Environmental Systems Division, 1971.

7. Detection of Solder Joint Imperfections. Autonetics Division, North American Aviation, January, 1965.

8. Development of Nondestructive Testing Techniques for Soldering Electrical Interconnections. Final Report, Martin Marietta Corporation, August, 1970.

9. Nondestructive Testing of Soldered Joints and Electronic Circuit Board Components. Progress Report, Quality Evaluation Laboratory, Naval Weapons Station, Concord, California, QE/CO 64-14, March, 1964.

10. Chuang, K. C.; and Marom, E.: Feasibility of Using Optical Correlation Techniques for Detecting Impending Fatigue Failure. Final Report, U.S. Army Aviation Laboratories, Fort Eustis, Virginia, April, 1969.

11. Chuang, K. C.: Materials Evaluation, vol. 26, no. 6, 1968, p. 116.

12. Chuang, K. C.; and Mueller, R. K.: Materials Evaluation, vol. 27, no. 4, 1969, p. 76.

13. Marom, E.: Laser Focus, vol. 5, no. 19, 1969, p. 43.

14. Jenkins, R.: Holographic Instrumentation Applications. Proceedings of a Conference held at Ames Research Center, Moffett Field, California, NASA SP-248, January 13-14, 1970.

REFERENCES (Concluded)

15. Collier, R. J.; Burckhardt, C. B.; and Lin, L. H.: Optical Holography. Academic Press, New York, N.Y., 1971.

16. Smith, A. M.: Principles of Holography. John Wiley and Sons, New York, N.Y., 1969.

17. Lamberts, R. L.; and Kurtz, C. N.: Applied Optics, vol. 10, 1971, p. 1342.

18. Korn, G. A.; and Korn, T. M.: Mathematical Handbook for Scientists and Engineers. McGraw-Hill Book Company, New York, N.Y., 1961.

19. Meyerhofer, D.: RCA Review, vol. 33, 1972, p. 110.

20. Shulman, A. R.: Optical Data Processing. John Wiley and Sons, New York, N.Y., 1970.

21. Douklias, N.; and Shamir, J.: Applied Optics, vol. 12, 1973, p. 364.

22. Manko, H. H.: Solder and Soldering. McGraw-Hill Book Company, New York, N.Y., 1964.

23. Standard Parts Mounting Design Requirements for Soldered Printed Wiring Board Assemblies. Marshall Space Flight Center, National Aeronautics and Space Administration, MSFC-STD-136, June 11, 1971.

24. Keller, J. D.: Papers on Soldering. American Society for Testing and Materials, New York, N.Y., 1962.

25. Foster, F. G.: Papers on Soldering. American Society for Testing and Materials, New York, N.Y., 1962.

26. Metals Handbook, Volume 1. American Society for Metals, Metals Park, Ohio, 1961.

NASA-Langley, 1975

"The aeronautical and space activities of the United States shall be conducted so as to contribute . . . to the expansion of human knowledge of phenomena in the atmosphere and space. The Administration shall provide for the widest practicable and appropriate dissemination of information concerning its activities and the results thereof."

—NATIONAL AERONAUTICS AND SPACE ACT OF 1958

NASA SCIENTIFIC AND TECHNICAL PUBLICATIONS

TECHNICAL REPORTS: Scientific and technical information considered important, complete, and a lasting contribution to existing knowledge.

TECHNICAL NOTES: Information less broad in scope but nevertheless of importance as a contribution to existing knowledge.

TECHNICAL MEMORANDUMS: Information receiving limited distribution because of preliminary data, security classification, or other reasons. Also includes conference proceedings with either limited or unlimited distribution.

CONTRACTOR REPORTS: Scientific and technical information generated under a NASA contract or grant and considered an important contribution to existing knowledge.

TECHNICAL TRANSLATIONS: Information published in a foreign language considered to merit NASA distribution in English.

SPECIAL PUBLICATIONS: Information derived from or of value to NASA activities. Publications include final reports of major projects, monographs, data compilations, handbooks, sourcebooks, and special bibliographies.

TECHNOLOGY UTILIZATION PUBLICATIONS: Information on technology used by NASA that may be of particular interest in commercial and other non-aerospace applications. Publications include Tech Briefs, Technology Utilization Reports and Technology Surveys.

Details on the availability of these publications may be obtained from:

SCIENTIFIC AND TECHNICAL INFORMATION OFFICE

NATIONAL AERONAUTICS AND SPACE ADMINISTRATION

Washington, D.C. 20546